JAMES Journal of Advances in Modeling Earth Systems®

RESEARCH ARTICLE
10.1029/2021MS002756

Key Points:

- The new ELM-Erosion model that represents cropland management and geological factors reproduce global soil erosion and sediment flux
- Our simulation shows that conservation agriculture has greatly reduced soil erosion in well-adopted countries, such as USA and Argentina
- Our result indicates that deforestation will increase sediment flux rapidly in tropical river basins of large rainforest coverage

Supporting Information:

Supporting Information may be found in the online version of this article.

Correspondence to:

Z. Tan,
zeli.tan@pnnl.gov

Citation:

Tan, Z., Leung, L. R., Li, H.-Y., & Cohen, S. (2022). Representing global soil erosion and sediment flux in Earth System Models. *Journal of Advances in Modeling Earth Systems*, *14*, e2021MS002756. https://doi.org/10.1029/2021MS002756

Received 5 AUG 2021
Accepted 14 DEC 2021

Author Contributions:

Conceptualization: Zeli Tan, L. Ruby Leung
Formal analysis: Zeli Tan
Funding acquisition: L. Ruby Leung
Methodology: Zeli Tan
Project Administration: L. Ruby Leung
Resources: Sagy Cohen
Software: Zeli Tan
Validation: Zeli Tan
Visualization: Zeli Tan
Writing – original draft: Zeli Tan
Writing – review & editing: L. Ruby Leung, Hong-Yi Li, Sagy Cohen

Representing Global Soil Erosion and Sediment Flux in Earth System Models

Zeli Tan[1], L. Ruby Leung[1], Hong-Yi Li[2], and Sagy Cohen[3]

[1]Pacific Northwest National Laboratory, Richland, WA, USA, [2]Department of Civil and Environmental Engineering, University of Houston, Houston, TX, USA, [3]Department of Geography, University of Alabama, Tuscaloosa, AL, USA

Abstract Soil erosion produces enormous amounts of sediment, carbon, and nutrient fluxes from land to rivers, thus playing crucial roles in global biogeochemical cycles and food security. To predict soil erosion in the context of climate and land use changes, we explicitly parameterize cropland management actions (i.e., irrigation, conserved agriculture, and crop residue management) and geological factors (i.e., lithology and glacier) in the Energy Exascale Earth System Model (E3SM) soil erosion module. The erosion model is calibrated using a global-scale regionalized parameter calibration method. The spatial variabilities of the modeled and the Revised Universal Soil Loss Equation (RUSLE) based benchmark soil erosion are consistent across vegetation, climate and soil properties. Compared with independent data, our model shows a bias reduction in 59% of the observations relative to the RUSLE-based soil erosion, with 53% of the bias reduction exceeding 50%. This improvement is mainly due to a better representation of the topographic effect on soil erosion. Our results indicate that conserved agriculture practices have effectively reduced soil erosion in cropland by over 25% in the United States and Argentina. In contrast, irrigation has increased soil erosion in many Asian countries. For upland sediment flux, our model is consistent with the WBMsed benchmark data in inter-basin variability but could be more skillful in simulating intra-basin variability because it couples soil erosion and sediment flux explicitly. The developed model provides useful skills for more realistic predictions of soil erosion and river sediment dynamics under environmental changes.

Plain Language Summary Soil erosion plays a crucial role in global biogeochemical cycles and food security but is rarely represented in climate models. To predict soil erosion in the context of climate and land use changes, we represent the effects of cropland management practices on soil erosion in the Energy Exascale Earth System Model (E3SM) soil erosion module. Our model demonstrates good performance in simulating the spatial variability of global soil erosion and upland sediment flux. Particularly, our simulations show that conserved agriculture practices have effectively reduced soil erosion in cropland by over a quarter in the United States and Argentina. In contrast, irrigation has increased soil erosion in cropland greatly in many Asian countries, such as India and China. Our simulations also show that deforestation will increase sediment flux in tropical rainforest watersheds rapidly. The developed model provides useful skills for more realistic predictions of soil erosion and river sediment dynamics in response to environmental changes.

1. Introduction

Soil erosion is an important land process that greatly shapes the topography, land cover, hydrology, and biogeochemistry of the Earth system (Berhe et al., 2018; Sobolev & Brown, 2019). Particularly, by transporting minerals, carbon, and nutrients from land to rivers (Galy et al., 2015; Tan et al., 2017), soil erosion alters the global carbon and nutrient cycles (Dialynas et al., 2016; Tan et al., 2020, 2021; Van Oost et al., 2007; Z. Wang et al., 2017), disturbs aquatic and coastal ecosystems (Blum & Roberts, 2009; Davies-Colley & Smith, 2001), and threatens agricultural sustainability (Lal, 2004; Montgomery, 2007). Historically, humans have increased soil erosion substantially through the expansion of agriculture (Jenny et al., 2019; Syvitski et al., 2005), while recent reforestation efforts, as well as conserved agriculture (CA), have helped to revert the increasing trend in many countries (Lal, 2004; Lanckriet et al., 2012; L. Li et al., 2020). Although soil erosion is ubiquitous and important, its interaction with climate change and the influence of soil erosion management actions on aquatic species protection and wetland restoration have not been well understood (Adams et al., 2020; Borrelli et al., 2020; Davies-Colley & Smith, 2001; L. Li et al., 2020; Lugato et al., 2018; Powlson et al., 2014; Tan et al., 2021). This limited understanding is partly because soil erosion is seldom represented in Earth System Models (ESMs), which is the primary tool to study climate change. As a result, it was usually studied as a standalone process rather than as a key element of the Earth system that interacts with the atmosphere, rivers, and oceans, and the two-way feedbacks between soil erosion and the global carbon cycle were ignored in the latest Intergovernmental Panel on Climate Change (IPCC) report (Denman et al., 2007).

The history of soil erosion and sediment flux (defined as the amount of detached sediment that reaches river networks) model development has been well documented in recent literature reviews (Batista et al., 2019; Borrelli et al., 2021; de Vente & Poesen, 2005; de Vente et al., 2013). Existing models differ significantly in structures (e.g., regression, factorial scoring, conceptual, and process-based), spatial scales (e.g., plot, hillslope, catchment, watershed, and continental), represented processes (e.g., interrill erosion, rill erosion, tillage erosion, gully erosion, deposition, and landslides), and focused land covers (e.g., cropland, rangeland, and woodland). Since ESMs are usually run at coarse spatial resolutions globally including remote regions, process-based soil erosion models at the catchment scale representing sediment deposition in all major land covers, with low to medium requirements for input data, would be favored (Tan et al., 2018). For example, based on comparison of eight representative soil erosion models over US catchments, we showed that the Morgan-Morgan-Finney model (Morgan & Duzant, 2008), although simple in formulations, is capable of representing soil erosion and sediment flux in diverse environments (Tan et al., 2018, 2020). We thus implemented it in the Energy Exascale Earth System Model (E3SM) land model (ELM), forming the ELM soil erosion model (ELM-Erosion).

As described in Tan et al. (2020), ELM-Erosion simplifies catchment-scale soil erosion and sediment flux processes into rainfall-driven erosion, runoff-driven erosion, and sediment transport capacity. These three processes are driven by E3SM simulated hydrological (i.e., throughfall, leaf drips and surface runoff) and ecological conditions (i.e., leaf area index, canopy height and land cover), both varying spatially and temporally, and geographic data (e.g., slope and soil texture) that only vary spatially. Despite its good performance in the US, our previous analysis also highlighted several aspects in ELM-Erosion that need to be improved to represent soil erosion and sediment flux realistically in the context of climate and land use change. These aspects include: (a) the effects of conserved tillage, plant residue management and irrigation on soil erosion, (b) full coupling of E3SM soil erosion, crop and dynamic land use models, and (c) a globally consistent parameter calibration scheme (Tan et al., 2018, 2020, 2021).

To achieve globally consistent modeling of soil erosion and sediment flux in ESMs, in this study, we will represent several important governing factors missing in the current ELM-Erosion and implement a global-scale regionalized parameter calibration method. Differences between ELM-Erosion simulation and benchmark data and model uncertainty will be analyzed to understand their environmental dependence. In addition, ELM-Erosion simulated soil erosion will be validated against independent datasets. Importantly, we will use ELM-Erosion to produce a global-scale 0.5-deg resolution map of sediment delivery ratio (SDR; the ratio of sediment flux to soil erosion), which could provide very useful information on the response of upland sediment, carbon, and nutrient fluxes to climate and land use change.

2. Methods and Materials

2.1. Model Description

Compared with Tan et al. (2018, 2020), the ELM-Erosion model is improved here to achieve consistent global modeling of upland soil erosion and sediment flux. In particular, we implement several changes to ELM-Erosion to better represent the impact of cropland management actions (i.e., irrigation, conserved tillage and managed plant residue), land use and land cover change (LULCC) and geology (i.e., glacier and lithology) on soil erosion and sediment flux. For cropland management actions, we enable the coupling of ELM-Erosion and the E3SM crop model and irrigation model (Leng et al., 2017; Zhou et al., 2020) and treat the irrigation water as an additional rainfall source for soil erosion. We also incorporate the CA factor for soil erosion into ELM-Erosion (Tan et al., 2017) and refine the plant residue effect on soil erosion using the scheme adopted by the Revised Universal Soil Loss Equation (RUSLE) model (Lippe et al., 2014; Renard et al., 1997). For LULCC, we enable the coupling of ELM-Erosion and the E3SM dynamic land use model which updates plant and soil water, carbon and nutrient budgets at the start of each year (Drewniak et al., 2015). For geological effects, we incorporate the glacier and lithology factors introduced by the BQART model (Syvitski & Milliman, 2007). The updated equations of ELM-Erosion are given below.

ELM-Erosion defines soil erosion as the sum of rainfall-driven erosion F and runoff-driven erosion H and upland sediment flux as the amount of detached sediment reaching the river network. As such, sediment flux is calculated as the lesser value of soil erosion and sediment transport capacity of overland flow T_c. Soil erosion by raindrops F is calculated as:

$$F = c_1 \times K \times P_{CA} \times L \times GC \times (KE_{DT} + KE_{LD}), \tag{1}$$

where K is the soil erodibility (kg J^{-1}), P_{CA} is the CA factor ($P_{CA} = 2.7$ if no cropland in a land unit is under CA and $P_{CA} = 1$ if 100% of cropland in a land unit is under CA), L is the lithology erodibility index that is the highest for unconsolidated sediments and the lowest for acid plutonic rocks (Moosdorf et al., 2018), GC is the ground cover factor that represents the reduction of erosion by plant residue and roots (Renard et al., 1997; Smets et al., 2008), and c_1 is a free parameter for the adjustment of rainfall-driven erosion due to deviation from the standard condition of soil texture, vegetation and rain regimes. The total energy of the effective rainfall (J m^{-2}) is the sum of the kinetic energy of the direct throughfall KE_{DT} and the leaf drainage KE_{LD} from both natural rainfall and anthropogenic irrigation. KE_{DT} is determined as a function of the rainfall intensity I (mm h^{-1}) and the effective rainfall reaching the ground surface:

$$KE_{DT} = R \times [(1 - CC) + CC \times (1 - A)] \times (11.87 + 8.73 \times \log_{10}(I)), \tag{2}$$

where R is total rainfall (mm), A is the fraction of the rainfall intercepted by the vegetation or canopy cover, and CC is the canopy cover fraction. And KE_{LD} is estimated by:

$$KE_{LD} = R \times CC \times A \times DR \times (15.8 \times PH^{0.5} - 5.87), \tag{3}$$

where PH is the height of the plant canopy (m) and DR is the fraction of leaf drainage.

Soil erosion by overland flow H (kg m^{-2}) is calculated as a function of surface runoff R_s (mm):

$$H = 19.1 \times c_2 \times Z \times P_{CA} \times L \times I_g \times GC \times R_s^{1.5} \times \sin\theta, \tag{4}$$

where Z is soil detachability by runoff (kg mm^{-1}), I_g is the BQART glacier erosion factor ($I_g = 1 + 0.09 \times A_g$, where A_g is the areal fraction (%) of glaciers in a grid cell), θ is slope angle, and c_2 is a free parameter for the adjustment of runoff-driven erosion due to deviation from the standard condition of soil texture, vegetation and rain regimes. The above equation assumes that soil particle detachment by runoff only occurs where soil is not protected by ground cover. For loose, non-cohesive soils (e.g., sand), $Z = 10^{-3}$. For cohesive soils, Z is calculated as $Z = 1/0.5 \times \mathrm{COH}$, where COH is the cohesion of the soil (Pa). The values of K and COH for different pfts and soil texture types are described in Tan et al. (2018).

The sediment transport capacity of overland flow T_c (kg m^{-2}) is given by:

$$T_c = 0.0191 \times c_3 \times SR \times P_{CA} \times L \times I_g \times R_s^2 \times (\sin\theta)^{1.25}, \tag{5}$$

where SR is the surface roughness factor, and c_3 is a free basin-specific parameter for the adjustment of transport capacity due to deviation from the standard condition of surface roughness, drainage density and rain regimes. The exponent of 1.25 for the slope factor is used following Pelletier (2012).

The ground cover factor GC in Equations 1 and 4 is defined as a function of ground cover and the root biomass density at the topsoil (the top inch of the soil column) (Renard et al., 1997; Smets et al., 2008):

$$GC = e^{-b_C \times \max(C_r, C_{\mathrm{LAI}}) - b_R \times B_R}, \tag{6}$$

where C_r is the surface cover fraction calculated from the plant residue, C_{LAI} is the surface cover fraction calculated from leaf area index (LAI) (Pelletier, 2012), B_R is the root biomass density at the topsoil (kg m^{-3}), and b_C and b_R are plant functional type (pft)-specific parameters for the effectiveness of surface cover and roots in reducing soil erosion, respectively. Noticeably, the values of b_C and b_R are different for rainfall- and runoff-driven erosion because roots are more effective in reducing runoff-driven erosion (Smets et al., 2008). Thus, we define b_{C1} and b_{C2} for the effectiveness of surface cover for rainfall-driven and runoff-driven erosion, respectively, and b_{R1} and b_{R2} for the effectiveness of roots for rainfall-driven and runoff-driven erosion, respectively. To convert plant residue biomass on the ground B_r (kg m^{-2}) to surface cover fraction C_r, we use the widely used exponential

Table 1
Summary of Numerical Experiment Settings

Numerical experiment	CA	LULCC	Irrigation	Glacier
Full experiment	Yes	Yes	Yes	Yes
No-CA experiment	No	Yes	Yes	Yes
No-irrigation experiment	Yes	Yes	No	Yes
No-glacier experiment	Yes	Yes	Yes	No
No-CA-LULCC experiment	No	No	Yes	Yes

relationship (Smets et al., 2008): $C_r = 1 - e^{-a \times B_r}$, where a is a regression coefficient that we set as 6.680 for the residue of all pfts. The use of a uniform a value is due to two reasons. First, differences in the effect of vegetation residue on soil erosion between different pfts are still being debated (X. Li et al., 2014; Smets et al., 2008). Second, the use of a uniform value simplifies the calibration of the parameter b_C which probably covaries with a. The surface roughness factor SR in Equation 5 is defined as a function of Manning's coefficient n (Misra & Rose, 1996):

$$SR = \left(\frac{0.03}{n}\right)^{0.6}, \tag{7}$$

where n is calculated as $n = 0.03 + 0.05 \times \max(C_r, C_{\mathrm{LAI}})$ (Lippe et al., 2014). In ELM-Erosion, the surface roughness factor SR varies both spatially and temporally.

2.2. Model Data and Simulation

The model was configured globally at 0.5-deg resolution for transient simulations from 2000 to 2014 using the Global Soil Wetness Project (GSWP) reanalysis forcing (Dirmeyer et al., 2006). To simulate the effect of LULCC on soil erosion, we used the LULCC data from the Land Use Harmonized version 2 (LUH2) transient data set (Hurtt et al., 2011) which was converted to 24 ELM pfts including a bare ground pft, 14 natural vegetation pfts and 10 crop pfts. The 10 crop pfts include five rainfed crop pfts (e.g., corn, cereal, soybean and generic crop) and five irrigated crop pfts (e.g., corn, cereal, soybean and generic crop). For irrigated crop pfts, the irrigation timing and amount are simulated by the ELM irrigation model which was first introduced by Sacks et al. (2009) based on soil moisture deficit and later enhanced by Leng et al. (2017) and Zhou et al. (2020) considering groundwater pumping and the balance of irrigation water demand and supply. The biomass of plant residue and roots are updated by ELM based on the dynamics of photosynthesis, respiration, phenology (planting, leaf emergence, grain fill and harvest) and carbon allocation (Drewniak et al., 2015; Oleson et al., 2013). To calculate the P_{CA} factor, we used the global-scale CA map of Prestele et al. (2018) and the United States (US) county-level tillage data compiled by the Conservation Technology Information Center (CTIC, 2008), as shown in Figure S1 of Supporting Information S1. The data of Prestele et al. (2018) was used for all regions except the conterminous US for which the more accurate CTIC data was used. Following Moosdorf et al. (2018), the lithology erodibility index L was calculated based on a global 0.5-deg resolution lithology map (Hartmann & Moosdorf, 2012), as shown in Figure S2 of Supporting Information S1.

To differentiate the effects of CA, irrigation, LULCC and glaciers on soil erosion, we set up five numerical experiments, as described in Table 1. Comparisons of the full versus no-CA experiments, the full versus no-irrigation experiments and the full versus no-glacier experiments are used to evaluate soil erosion changes caused by CA, irrigation, and glaciers, respectively. In addition, comparison of the full versus no-CA-LULCC experiments is used to evaluate the total impact of CA and LULCC on the Mississippi's upland sediment flux.

To analyze the effects of climate, vegetation, and topography on soil erosion, we used the following data: (a) mean annual temperature (MAT) and mean annual precipitation (MAP) from the WorldClim version 2.1 climate data (Fick & Hijmans, 2017), (b) gross primary production (GPP) from the data set of Jung et al. (2011), (c) cropland fraction from the LUH2 data set (Hurtt et al., 2011), and (d) elevation and slope from a 90 m resolution Digital Elevation Model (Lehner et al., 2008).

2.3. Model Calibration and Validation

ELM-Erosion has seven free parameters for calibration: c_1, c_2, c_3, b_{C1}, b_{C2}, b_{R1}, and b_{R2}. As described in Section 2.1, the values of these parameters are spatially correlated and usually depend on soil texture, pft and climate. Thus, it is reasonable to use a global-scale regionalized parameter calibration method for model calibration (Beck et al., 2016). First, because the parameters b_{C1}, b_{C2}, b_{R1}, and b_{R2} are pft-specific, they can be set to the same values for the same land cover. Second, for the parameters c_1 and c_2, because the uncertain factors K and Z are related to soil texture and land cover and the relationships of KE_{DT} and H to rainfall and runoff probably depend on climate regimes (Morgan & Duzant, 2008), they should vary with pft, soil texture and climate. Thus, the values of the

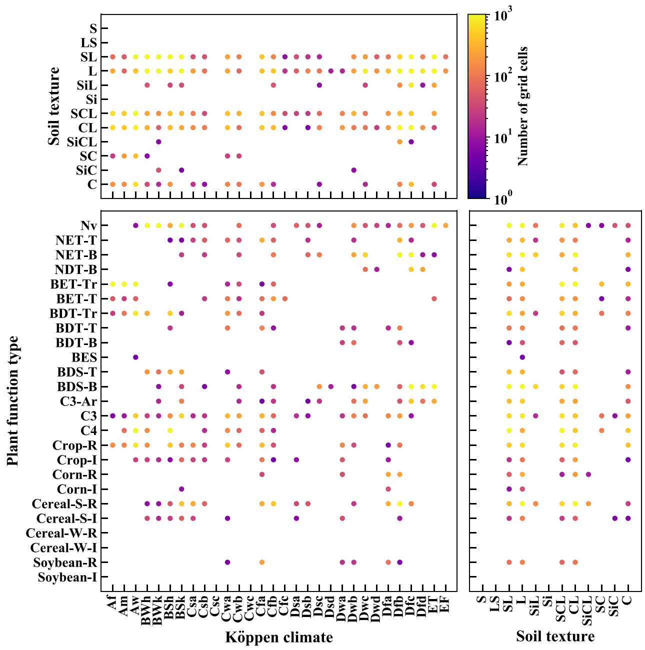

Figure 1. Distribution of the 0.5-deg resolution E3SM grid cells by pft, soil texture, and climate classification.

parameters c_1 and c_2 can be set to the same values for the same combination of pft, soil texture and the Köppen-Geiger climate classification. Third, the parameter c_3 can be calibrated for each river basin where pre-dam sediment flux data are available.

In theory, the parameters c_1 and c_2 should span over 25 pfts (Table S1 in Supporting Information S1), 12 soil texture types (Table S1 in Supporting Information S1), and 30 Köppen-Geiger types (Beck et al., 2018), which would correspond to 9,000 combinations in total. But after regionalization, only 679 combinations (or 7.5% of the total combinations) that have at least five corresponding grid cells (Figure 1) are needed to cover the grid cells globally. Thus, our global-scale regionalized calibration follows three steps: (a) running an ensemble of 4800 ELM-Erosion simulations with each simulation using different parameter values that are randomly sampled within the parameter space, (b) calculating the model bias of each model simulation for 679 combinations against the soil erosion benchmark data, and (c) applying a Monte-Carlo-based Bayesian recursive parameter optimization scheme (Tang & Zhuang, 2009) to select optimal values of c_1 and c_2 for each combination. To construct the probability density function of the parameters, we use an ensemble size of 4,800, which is a factor of 10 larger than the ensemble size needed for screen sensitivity analysis (Campolongo et al., 2007) calculated as $160 \times (N_{\text{param}} + 1)$ with the parameter number N_{param} equals to 2.

After calibrating b_{C1}, b_{C2}, b_{R1}, b_{R2}, c_1, and c_2, we ran another ensemble of 4800 ELM-Erosion simulations by varying c_3 values, calculated the model bias of each model simulation against the sediment flux benchmark data, and applied the Bayesian optimization scheme to select optimal c_3 values for each river basin.

The soil erosion benchmark data is derived from the RUSLE estimate of Borrelli et al. (2017), with soil erosion in China refined by the data set of Yue et al. (2016). The sediment flux benchmark data is derived from the WBMsed pre-dam (its "Pristine" mode) estimate (Cohen et al., 2014), with many refinements based on the published data of Milliman & Farnsworth (2011) and H. Wang et al. (2007). WBMsed is used to simulate global water discharge and suspended sediment flux over the same 0.5-deg resolution river network (WBMsed native simulation is 6 arc-minute) as ELM-Erosion but with different input data. Both the RUSLE and WBMsed models have been widely used and validated for long-term soil erosion and sediment discharge calculations, respectively (Cohen et al., 2013, 2014; Renard et al., 1997). Because WBMsed is developed to simulate sediment discharge in large rivers, we set the parameter c_3 to unity for rivers that only occupy a single grid cell. To validate the simulated soil erosion, we used the catchment-scale soil erosion data from Mishra et al. (2019) and the Global Applications of Soil Erosion Modeling Tracker (GASEMT) database (Borrelli et al., 2021). The data of Mishra et al. (2019) have been converted to $t\ km^{-2}\ yr^{-1}$ by multiplying them by the soil bulk density that is calculated in ELM based on soil porosity (Oleson et al., 2013). For the validation data, we mapped each record to the ELM 0.5-deg resolution grid and averaged the values by site areas if multiple records were mapped into the same grid cell.

3. Results

3.1. Global Soil Erosion Modeling

As expected, the calibrated model parameters show substantial spatial variabilities that are closely correlated with the variability of vegetation and climate (Figure 2). Because soil erosion is usually insensitive to the surface cover and root factors of rainfall-driven erosion b_{C1} and b_{R1} (Table S2 in Supporting Information S1), we mostly set their values for pfts by default. The values of the surface cover and root factors of runoff-driven erosion b_{C2} and b_{R2} are higher in areas with more vegetation biomass, such as tropical rainforest (Figure 2), which can be attributed to the better protection of surface cover and roots on soils in areas of dense vegetation. Except for deserts where water-driven soil erosion is negligible, the scaling factors of rainfall-driven and runoff-driven erosion c_1 and c_2 are lower in well-vegetated areas under various climates, such as tropical rainforest and boreal forest,

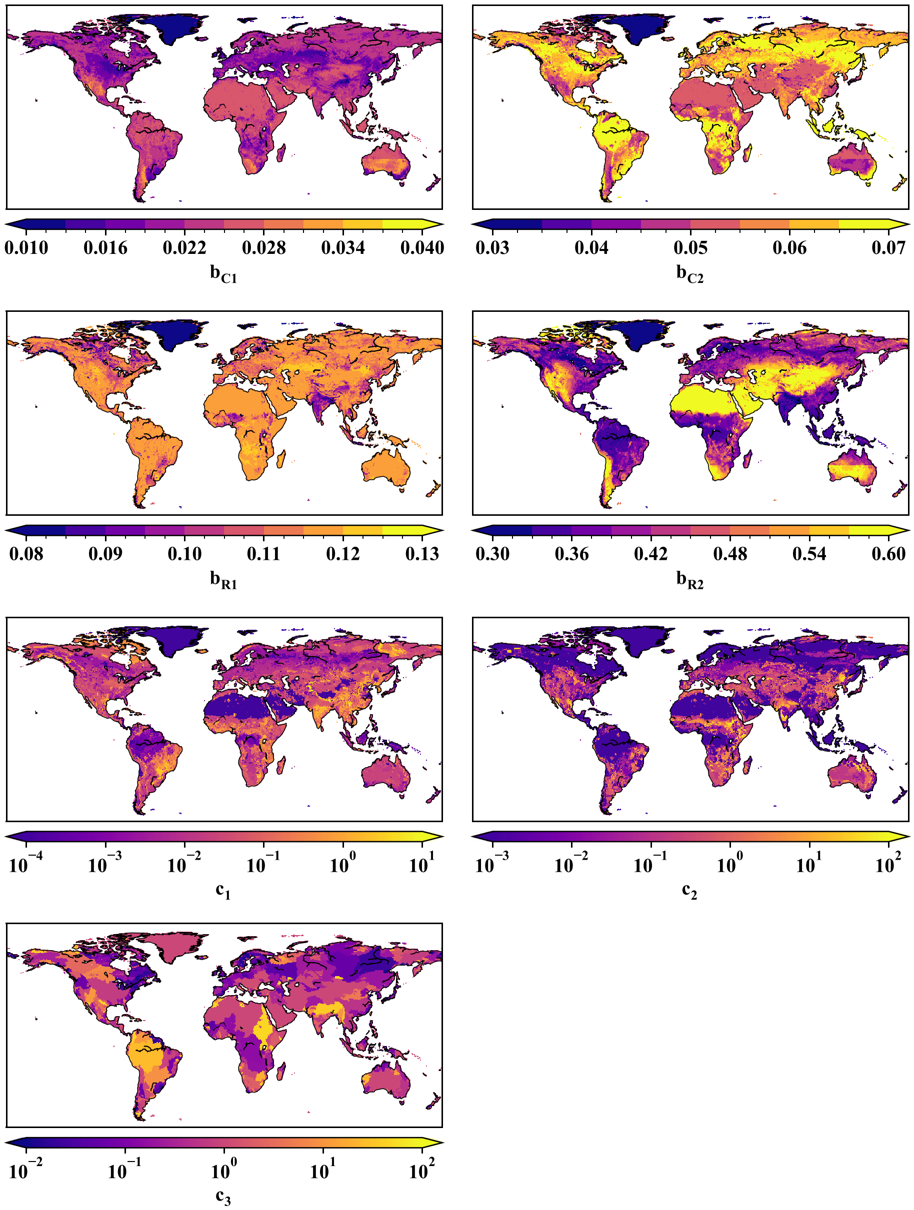

Figure 2. Global distribution of the calibrated ELM-Erosion parameters.

and higher in poorly vegetated areas with high precipitation, such as tropical and subtropical cropland (Figure 2), which is consistent with the spatial variability of the soil erosion benchmark (Borrelli et al., 2017). The spatial variability of the scaling factor of sediment transport capacity c_3 is less evident, because the calibration of c_3 is river basin based, and large river basins usually span several ecoclimate zones.

Through regionalized calibration, ELM-Erosion successfully reproduces the spatial variability of the soil erosion benchmark (Figure 3): the log-log linear regression between our simulation and the benchmark is $y = 1.13\ x^{0.95}$ with $R^2 = 0.825$ and $p < 0.0001$. Both ELM-Erosion and the benchmark data predict high soil erosion in areas of vast cropland, including the plains in China, India, US, and South America, or steep topography, including the Himalayas and Andes, and low soil erosion in areas of dense vegetation, including the tropical and boreal forest. Because of extremely low precipitation, soil erosion in desert areas, including the Sahara, Gobi, and Atacama Desert, is negligible. For US, Europe, India and South Africa, our simulated mean soil erosion rates in cropland are 597, 272, 726, and 517 t km^{-2} yr^{-1}, respectively, which are close to previous independent estimates, such as the estimate of 668 t km^{-2} yr^{-1} for US cropland by USDA (2018), the estimate of 246 t km^{-2} yr^{-1} for European

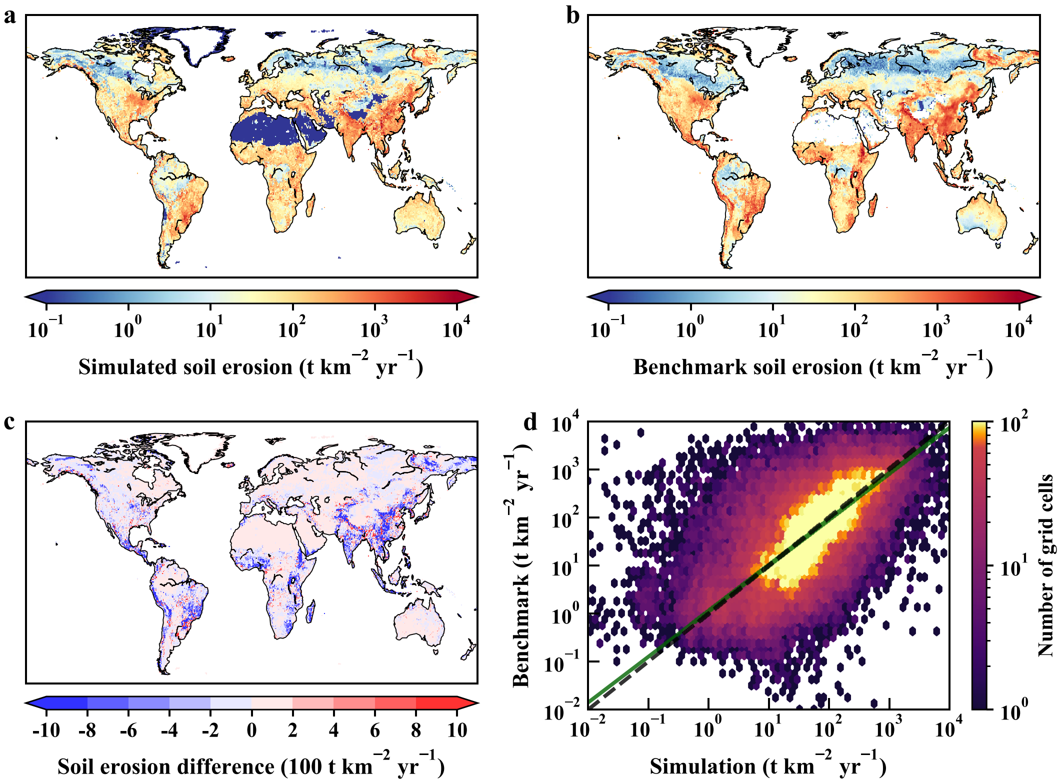

Figure 3. Global maps of the (a) simulated soil erosion, (b) the benchmark soil erosion, (c) the simulation-benchmark difference, and (d) scatterplot of the simulated versus benchmark soil erosion. In panel (d), the black dashed line is the 1:1 reference and the green line is the linear regression between simulation and benchmark ($y = 1.13\ x^{0.95}$ with $R^2 = 0.825$ and $p < 0.0001$).

cropland by Panagos et al. (2015), the estimate of 864 t km^{-2} yr^{-1} for Indian cropland by Doetterl et al. (2012), and the estimate of 690 t km^{-2} yr^{-1} for cropland in South Africa by Compton et al. (2010). Our simulated global soil erosion in cropland is 7.13×10^9 t yr^{-1}, which is within the range of the estimate ($13.1 \pm 6.6 \times 10^9$ t yr^{-1}) by Doetterl et al. (2012). Noticeably, ELM-Erosion achieves all these consistent estimates by using input data that are at much coarser resolutions and probably also have lower quality than those used in independent studies. For Australia, our simulated mean soil erosion rate in cropland is 168 t km^{-2} yr^{-1}, which is only half of the estimate (340 t km^{-2} yr^{-1}) by Lu et al. (2003). But Lu et al. (2003) also pointed out that for improved legumes and cereals, the major crops in Australia, the mean soil erosion rate is 190 t km^{-2} yr^{-1}. Thus, the large discrepancy between our estimate and Lu et al. (2003) is likely caused by the difference in land use data. For instance, the LUH2 data set used by ELM-Erosion does not differentiate some erosion-prone crops in Australia, such as sugarcanes (Lu et al., 2003).

As shown in Figure 4, the simulated and benchmark soil erosion rates are also comparable at the levels of pft, soil texture and climate classification. Consistent with observations (Lanckriet et al., 2012; Poesen & Savat, 1981; Poesen et al., 2003), soil erosion is greatly elevated in grid cells dominated by crop pfts, particularly under warm climate, which is mainly caused by weakened soil cohesion (e.g., high rain erodibility K and soil detachability Z) and vegetation protection by agricultural activities (e.g., low LAI). Soil erosion is also large in grid cells dominated by broadleaf evergreen shrub, which is usually located in hilly areas of the Mediterranean climate with strong seasonality (Vanmaercke et al., 2011). Comparison of soil erosion under different climates (Figure 4c) demonstrates the non-monotonic dependence of soil erosion on temperature and precipitation (García-Ruiz et al., 2015).

Because ELM-Erosion and RUSLE differ in the model parameterization, there still exist large differences between the two estimates in some regions, such as the Andes, the Brazilian Plateau, and the Yungui Plateau of China (Figure 3c), and for some pfts, such as tropical broadleaf evergreen tree (Figure 4a). Comparison of the ELM-Erosion and RUSLE-based soil erosion along gradients of climate, topography and vegetation reveals that

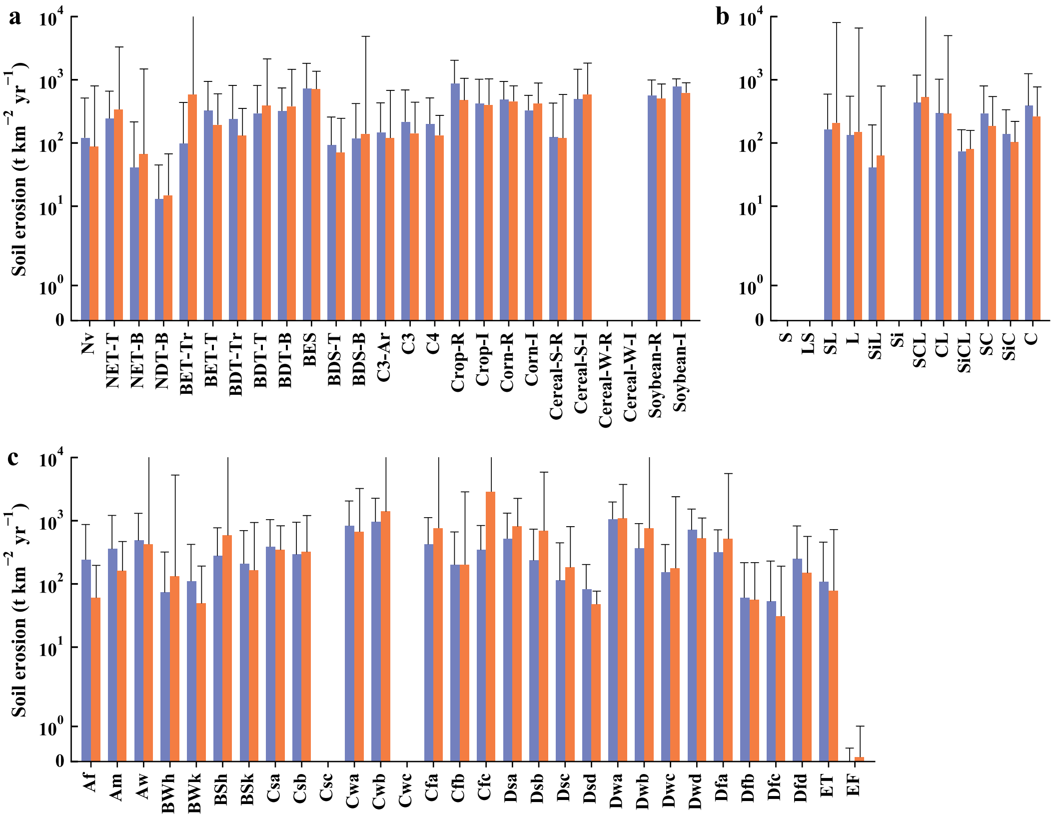

Figure 4. Comparison of the simulated soil erosion (orange) and the benchmark soil erosion (blue) over (a) Köppen climate classification, (b) pft, and (c) soil texture. Bar plots represent the mean and standard deviation values.

the difference between the two models could be mainly caused by their distinct parameterizations of soil erosion versus slope relationship (Figure 5): high Kling-Gupta efficiency (KGE) scores for consistent response of soil erosion to climate and vegetation variations and low KGE scores for divergent response of soil erosion to topography variations between the two models. ELM-Erosion predicts much weaker response of soil erosion to the increase of elevation and slope than that in RUSLE (Figures 5c–5d). For high-elevation (elevation >1,000 m) and high-slope (slope >3°) regions, the RUSLE-based estimate is much larger. This discrepancy could have two causes. First, because the RUSLE-based estimate is based on high-resolution slope data (Borrelli et al., 2017), it can represent more steep slopes in mountainous regions where intense soil erosion is produced during rain events. Second, RUSLE accounts for slope length in its slope factor that is difficult to calculate and has variable relationships with dominant erosion processes in regions of rough topography (Wu et al., 2021). Comparison of the ELM-Erosion and RUSLE-based estimates to observations indicates that the soil erosion versus topography relationship in ELM-Erosion could be more realistic (Figure 6). Compared to RUSLE, ELM-Erosion reduces soil erosion model bias at 59% of the observations (the total number of observations is 608), with 53% of the bias reduction exceeding 50%, and only increases model bias by over half at 17% of the observations. The relative bias of the ELM-Erosion simulated soil erosion is less than one in more than 70% of the observation sites, which is also better than RUSLE (Figure 6e). In particular, ELM-Erosion reduces soil erosion model bias substantially in the Andes, the Alps and the Yungui Plateau of China (Figure 6c). Comparison of the ELM-Erosion and RUSLE-based soil erosion bias along gradients of elevation and slope confirms that ELM-Erosion performs better in simulating soil erosion for mountainous regions with elevation larger than 1,000 m or slope larger than 3° (Figure 7).

ELM-Erosion also predicts lower soil erosion in areas of high cropland coverage than RUSLE (Figure 5f). Considering the robustness of RUSLE in modeling soil erosion in cropland, soil erosion is likely moderately underestimated by ELM-Erosion in cropland-dominated areas, as indicated in Figure 7f.

10.1029/2021MS002756

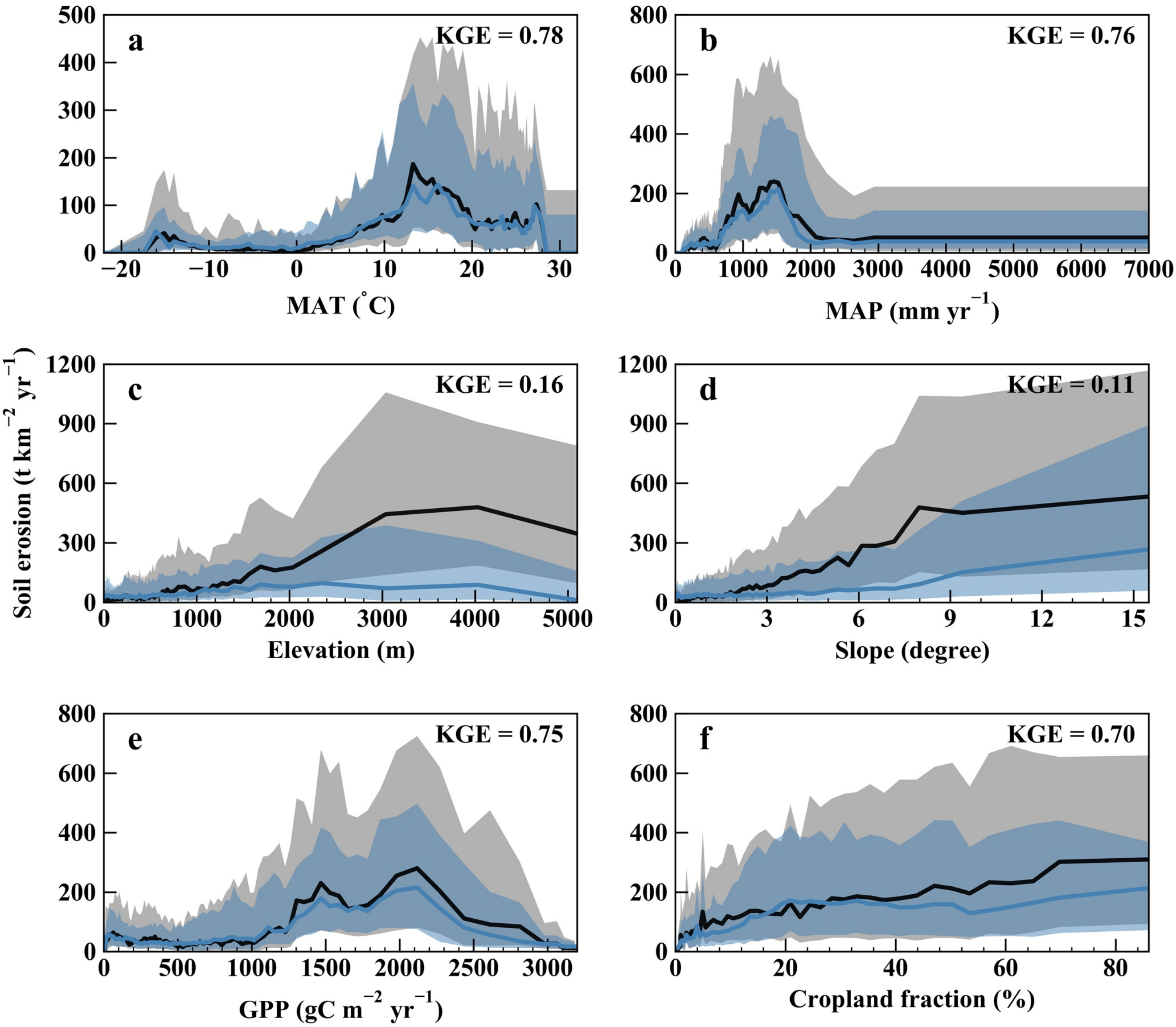

Figure 5. Comparison of the simulated (blue) and the benchmark (black) soil erosion over gradients of (a) MAT, (b) MAP, (c) elevation, (d) slope, (e) GPP, and (f) cropland fraction. Solid lines and shaded areas represent the median and the 25th and 75th percentiles of the simulated and benchmark soil erosion. The KGE scores are calculated based on the median values of the simulated and benchmark soil erosion.

In contrast, the dependence of ELM-Erosion modeled soil erosion on mean annual temperature (MAT) and precipitation (MAP) is very consistent with that in RUSLE, even though RUSLE skews toward higher values for some MAT and MAP regimes (Figures 5a–5b). This consistency possibly implies that both the rainfall erosivity factor of RUSLE and the rainfall and runoff factors of ELM-Erosion are robust in predicting the response of long-term soil erosion rates to climate variations. Comparison of the ELM-Erosion and RUSLE estimate biases along gradients of MAT and MAP also shows that there are no substantial differences in skills between the two models for different MAT and MAP regimes (Figures 7a–7b). Similarly, the dependence of soil erosion on gross primary production (GPP) is also consistent between ELM-Erosion and RUSLE (Figure 5e). Thus, the vegetation cover factors of both RUSLE and ELM-Erosion are robust in modeling the response of long-term soil erosion rate to vegetation variations (Figure 7e).

As shown in Figure 6, ELM-Erosion underestimates soil erosion in many tropical islands of intense seismic activities, such as those in Indonesia, Papua New Guinea, Philippines, and Taiwan. Further analysis using the data of seismic activities (Giardini et al., 1999) shows that the underestimation mainly occurs within the peak

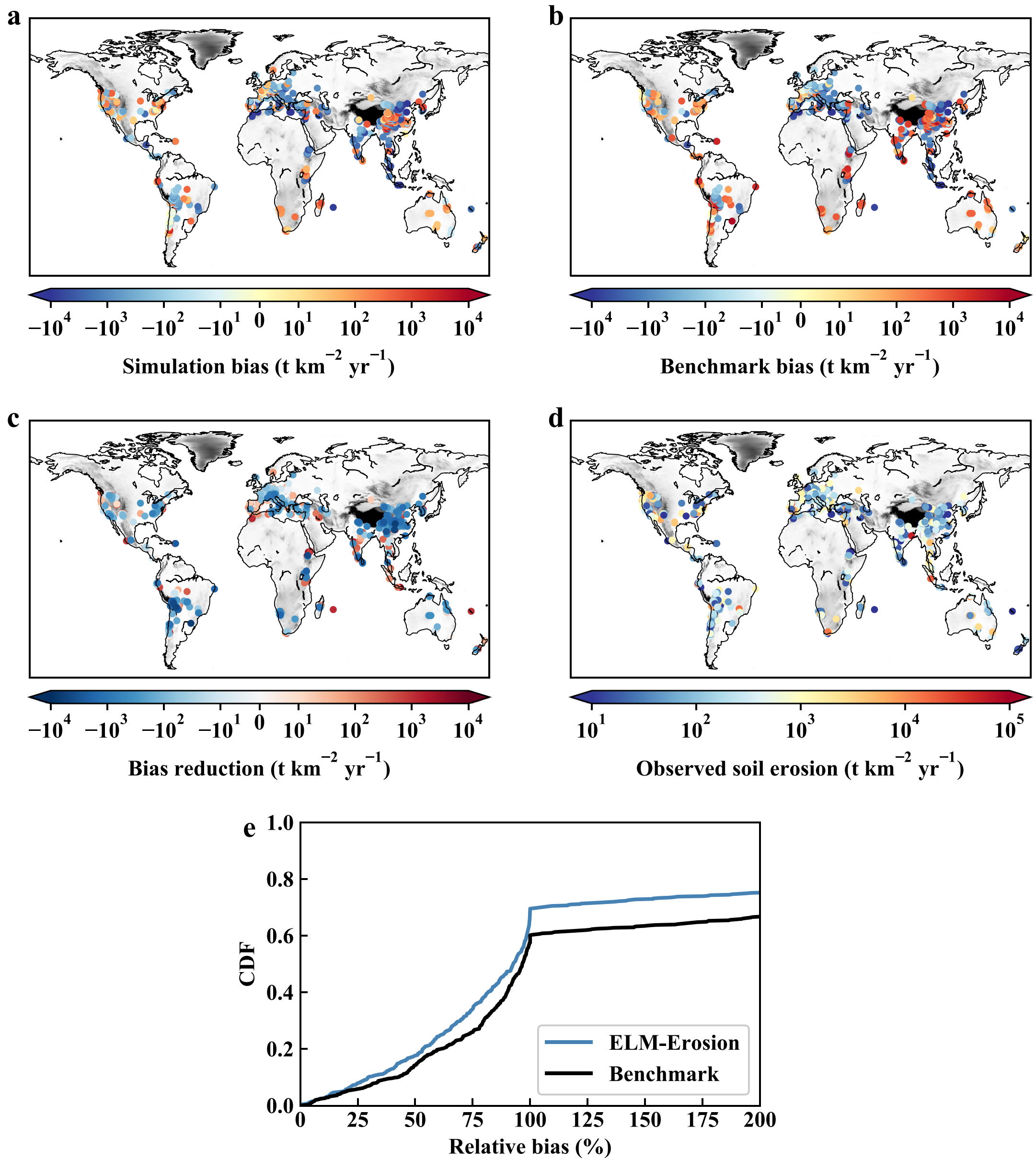

Figure 6. (a) Bias of the simulated soil erosion, (b) the RUSLE-estimated soil erosion, (c) comparison of the simulated and the RUSLE-estimated soil erosion bias, (d)the observed soil erosion, and (e) comparison of the cumulative distribution function (CDF) of the simulated and the RUSLE-estimated soil erosion relative bias. Dark gray in panels (a–d) represents high elevation.

ground acceleration (PGA) zone between 2 and 4 m s^{-1} (Figure S3 in Supporting Information S1). Because strong earthquakes usually trigger extensive landslides (Dadson et al., 2003), this model bias is likely caused by ignoring landslide-induced soil erosion in ELM-Erosion.

3.2. Impacts of CA, Irrigation, and Glaciers

Compared to the no-CA experiment, the full experiment that accounts for the effect of CA predicts much lower soil erosion in countries where CA practices are widely adopted (Figure 8). The effect of CA on soil erosion is particularly profound in the US Midwest and Argentina. Globally, US, Argentina and China rank top in using CA to reduce soil erosion. Our simulation results (Figure 8c) show that the adoption of various CA practices may have reduced the total soil erosion in US cropland from 1.28×10^9 t yr^{-1} to 0.93×10^9 t yr^{-1} and relatively

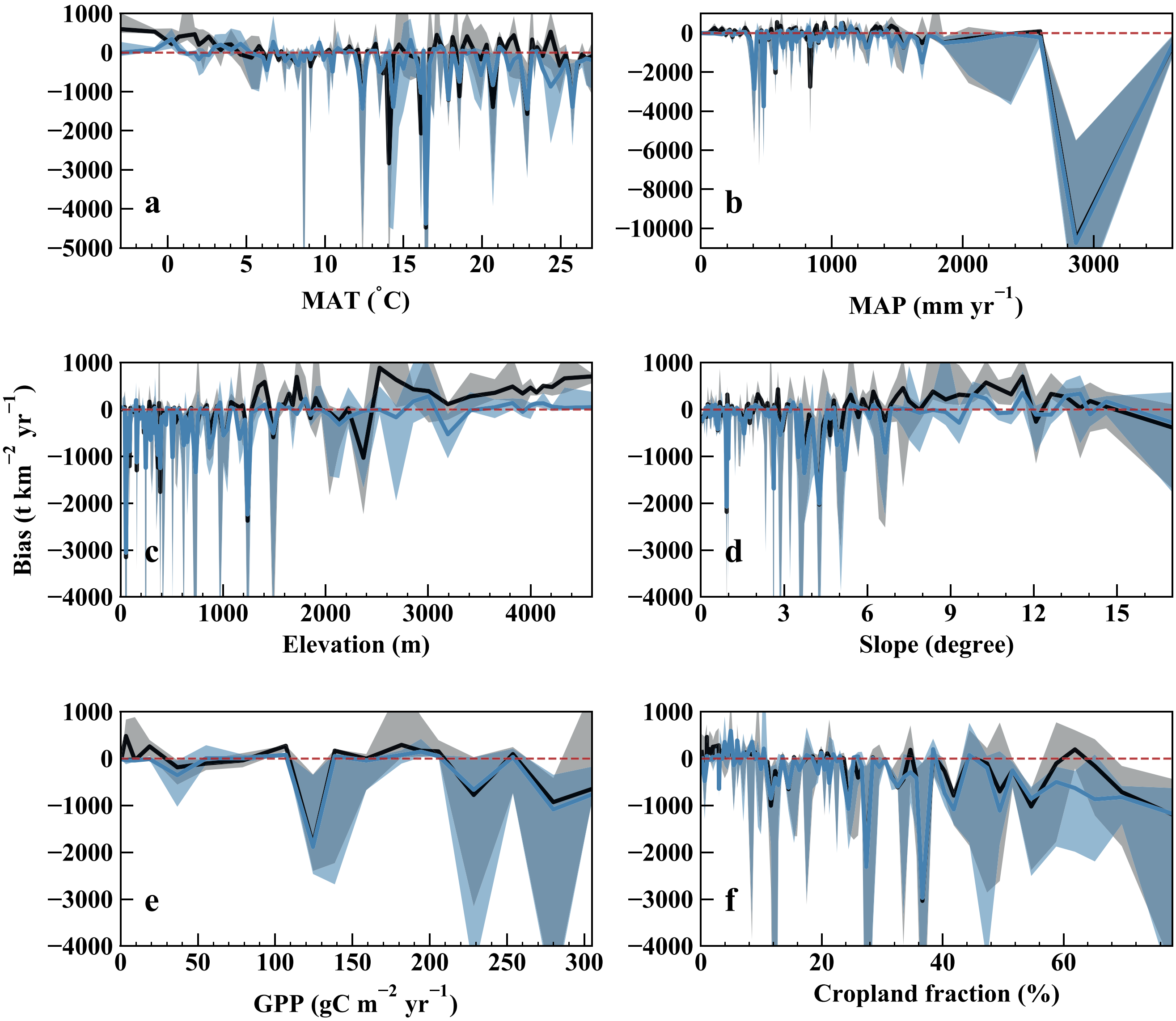

Figure 7. Comparison of the simulated (blue) and the RUSLE-estimated (black) soil erosion bias over gradients of (a) MAT, (b) MAP, (c) elevation, (d) slope, (e) GPP, and (f) cropland fraction. Solid lines and shaded areas represent the median and the 25th and 75th percentiles of the simulated and RUSEL-estimated soil erosion bias.

by 27%. Similarly, the adoption of CA practices may have reduced the total soil erosion in Argentinian cropland from 0.27×10^9 t yr^{-1} to 0.20×10^9 t yr^{-1} and relatively by 28%. Because of uncertainty in the CA data (Table S3 in Supporting Information S1), our estimate may have large uncertainties for some countries such as Brazil.

The effect of irrigation on soil erosion is the most pronounced in East and South Asia, especially China and India (Figure 9). By comparing the simulated soil erosion between the full experiment and the no-irrigation experiment, we find that irrigation may have increased the total soil erosion in cropland in China from 1.42×10^9 t yr^{-1} to 1.56×10^9 t yr^{-1} and relatively by 10%, with the largest increase in North China (Figure 9c). The effect of irrigation on soil erosion is even larger in India, with the increase of the total soil erosion in cropland from 1.06×10^9 t yr^{-1} to 1.18×10^9 t yr^{-1} and relatively by 12%. Globally, China, India, and US rank top for the amount of irrigation-induced soil erosion because they have the largest irrigation area and water usage in the world (Figure 9b). If measured by the soil erosion increase ratio, the effect of irrigation is even much larger in Egypt (Figure 9c) where the agricultural water demand is almost solely met by irrigation. The accuracy of our estimates could be limited because of uncertainties in the ELM irrigation model in estimating irrigation efficiency and water demand (Leng et al., 2017; Zhou et al., 2020).

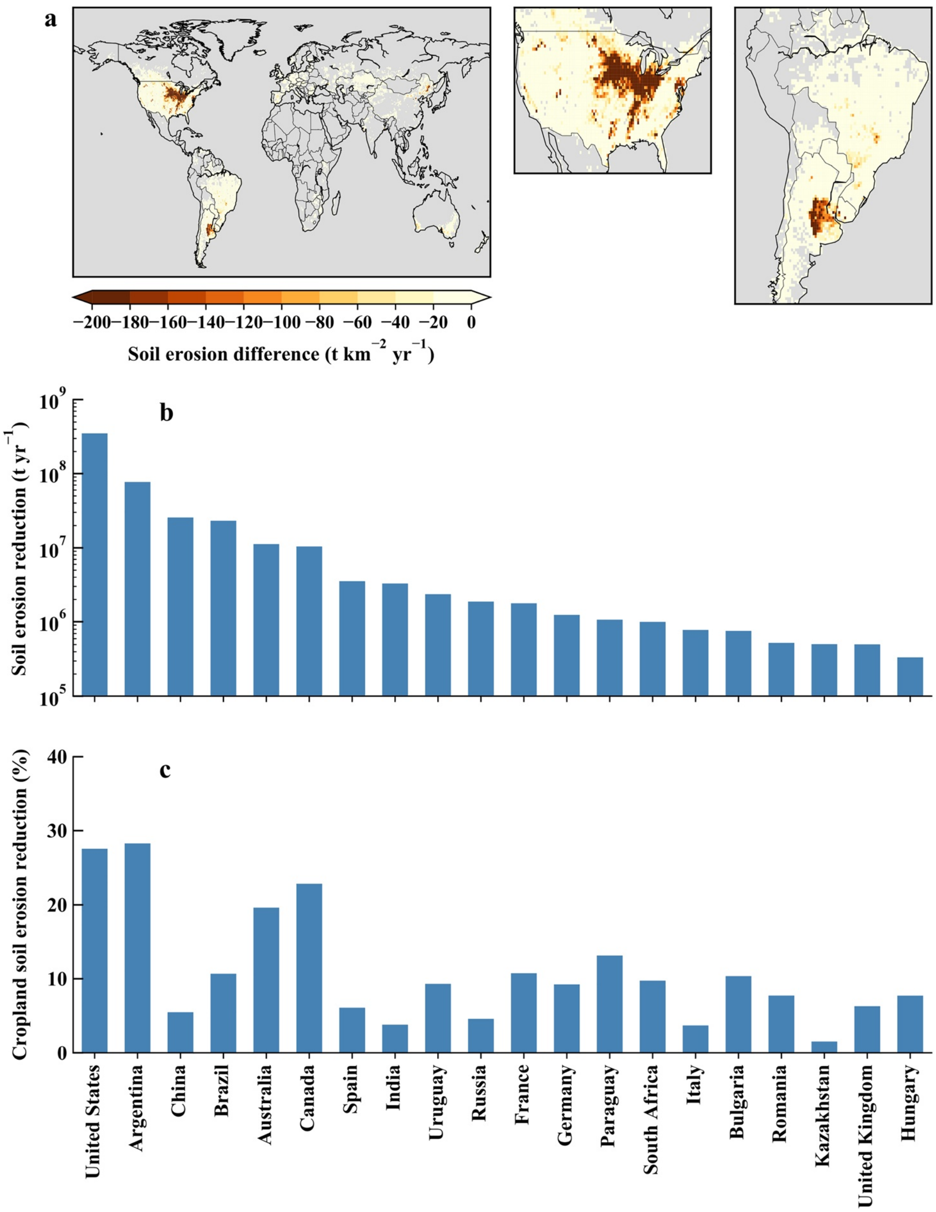

Figure 8. (a) Maps of CA-induced soil erosion reduction, (b) ranking of the total amount of CA-induced soil erosion reduction by country, and (c) the reduction ratio of soil erosion in cropland for the top ranked countries.

The effect of glaciers on soil erosion is minor at the global scale (Figure S4 in Supporting Information S1). But for some regions, such as the Himalayas, the Alps, and the Pacific Coast Ranges in Alaska and British Columbia, the increase of soil erosion induced by glacial movement is profound. Noticeably, our model likely underestimates glacier-induced soil erosion in Greenland and the Antarctic (Overeem et al., 2017) because ELM does not assign soil columns to many of the land grid cells in these permanently ice-covered regions.

3.3. Global Sediment Flux Modeling

ELM-Erosion and WBMsed are consistent in modeling inter-basin variability of sediment flux (Figure 10). Because ELM-Erosion couples soil erosion and sediment flux in upland explicitly, the spatial variability of soil erosion and sediment flux simulated by the model are highly correlated (Figures 3a and 10c). As shown in Figure 10d, the two models have a higher agreement at large river basins, possibly because WBMsed was developed

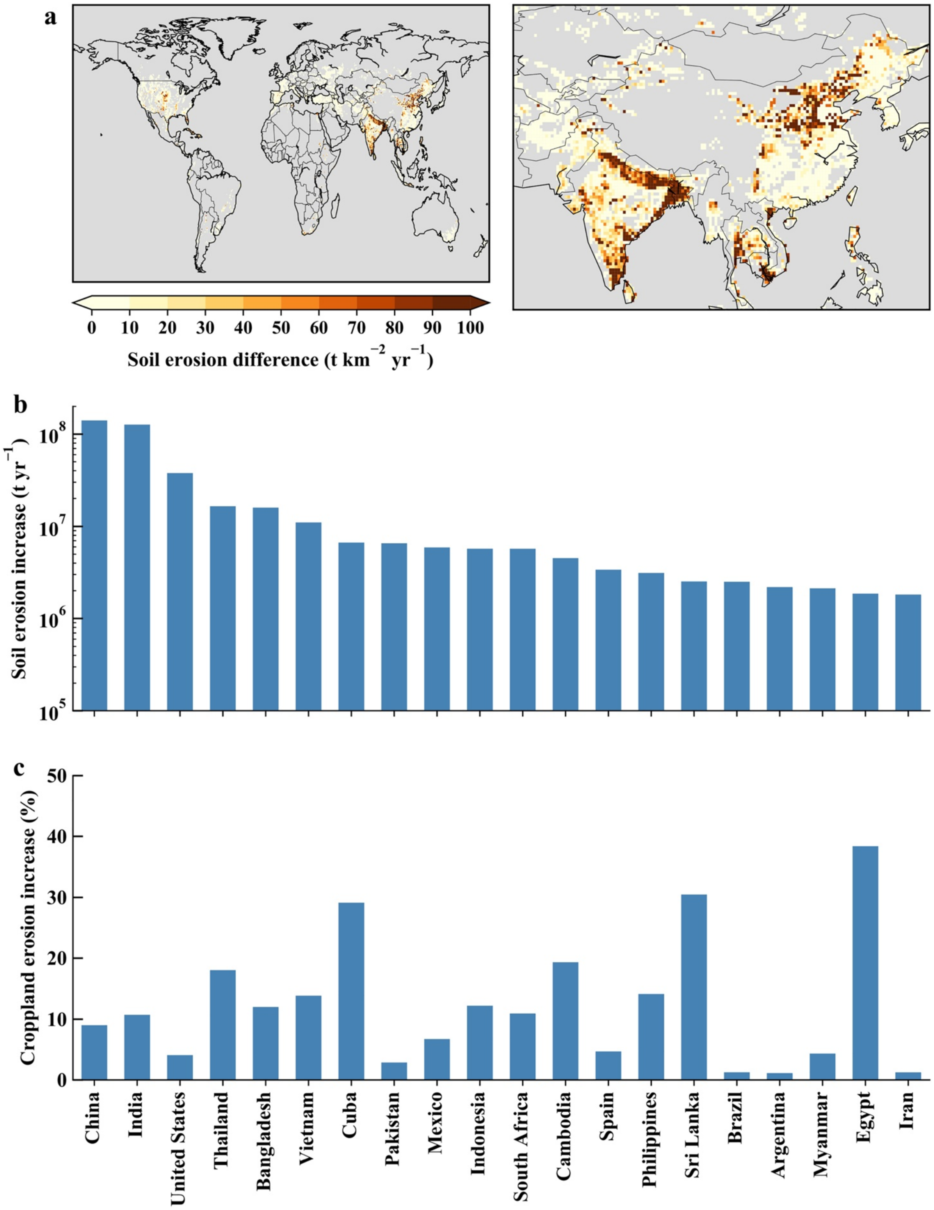

Figure 9. (a) Maps of irrigation-induced soil erosion increase, (b) ranking of the total amount of irrigation-induced soil erosion increase by country, and (c) the increase ratio of soil erosion in cropland for the top ranked countries.

to predict sediment discharge of large rivers and its uncertainty for small rivers could be substantial (Cohen et al., 2014). It should be noted that for some large rivers, such as the Yellow River, the difference between ELM-Erosion and WBMsed is caused by the refinement of pre-dam sediment discharge for calibration using the published data. Consistent with observations (Milliman & Farnsworth, 2011), the simulated global sediment flux is mainly contributed by large rivers in the tropics and subtropics, such as Amazon, Ganges, Paraná, Nile, Yangtze, Yellow, Mississippi, Indus, Mekong, Irrawaddy, and Congo. For many of these rivers, sediment flux from upland is crucial for sustaining the river deltas as important biodiversity hotspots, such as the Ganges delta, the Mississippi delta and the Mekong delta (Blum & Roberts, 2009; Lovelock et al., 2015).

Compared to WBMsed, ELM-Erosion may have improved the modeling of global sediment flux in several aspects (Figure 10). First, it eliminates unrealistic sediment flux hotspots at many exorheic or small river basins predicted by WBMsed, such as those in Figure S5b of Supporting Information S1. These unrealistic hotspots could be produced for two reasons: (a) the WBMsed hydrology module has large uncertainties in simulating

10.1029/2021MS002756

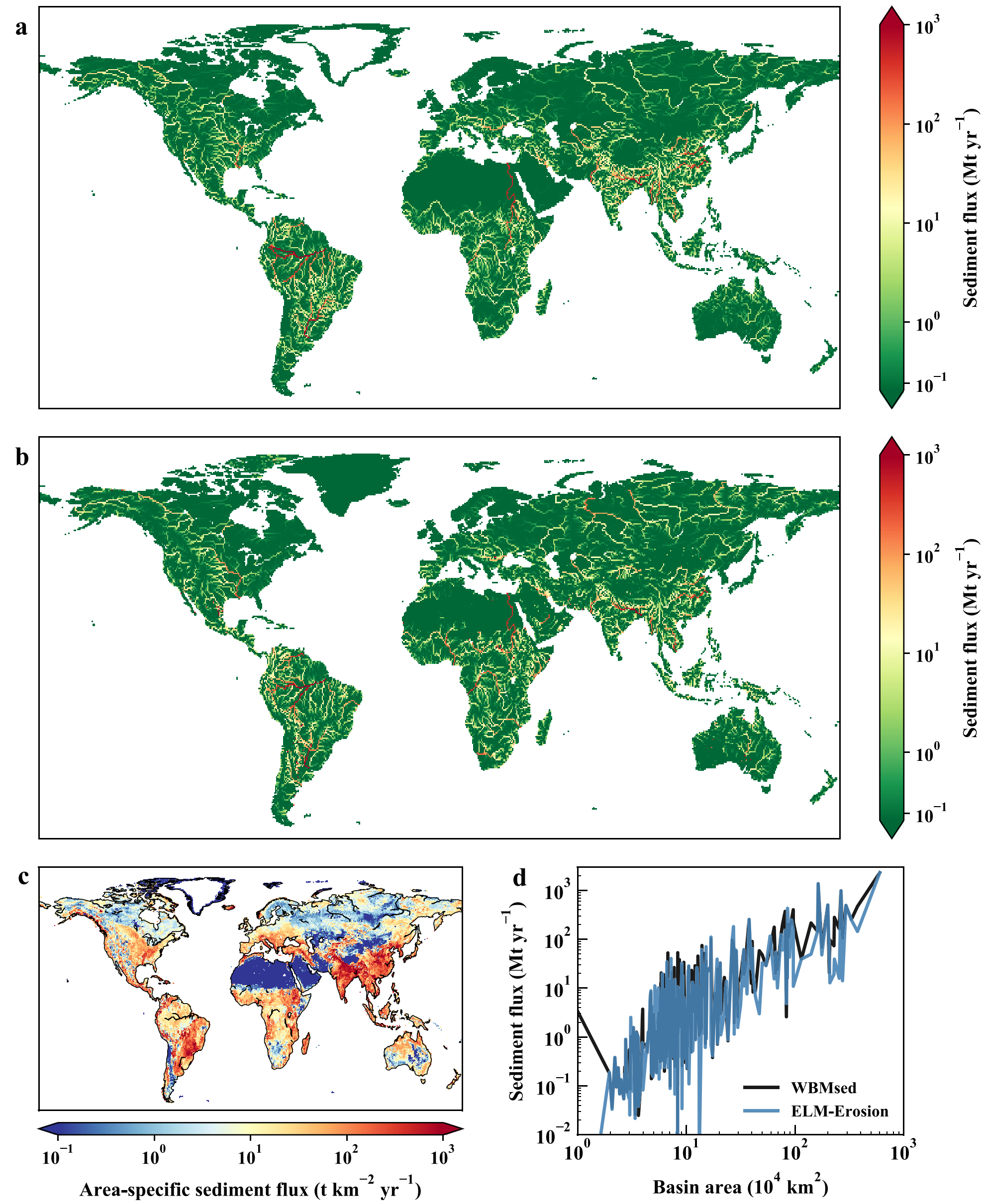

Figure 10. (a) Maps of the ELM-Erosion simulated basin-scale sediment flux, (b) the WBMsed simulated basin-scale sediment flux, (c) the ELM-Erosion simulated area-specific sediment flux from upland, and (d) comparison of the ELM-Erosion and the WBMsed simulated basin-scale sediment flux over gradient of river basin area. For each grid cell, basin-scale sediment flux is the accumulated sediment flux from its upstream catchment.

river discharge in exorheic river basins or headwater catchments and (b) the relationship between sediment flux and basin area used by WBMsed is inappropriate for small basins. Second, it better represents the intra-basin variability of sediment flux by coupling sediment flux and soil erosion explicitly. For example, in the Nile River, ELM-Erosion predicts a much larger sediment supply from its Blue Nile tributary (Figure S5 in Supporting Information S1). Given that Blue Nile flows through the erosion-prone Ethiopian Plateau and supplies over 80% of the water in the Nile during the rainy season (Awulachew et al., 2009), the ELM-Erosion prediction should be more plausible. Similarly, previous studies showed that the Ohio River supplies a large fraction of sediment in the Mississippi (Lee & Reutter, 2019), as predicted by ELM-Erosion (Figure S5 in Supporting Information S1).

Our calculation shows that sediment delivery ratio (SDR) has substantial inter- and intra-basin variabilities (Figure 11). For example, the estimated SDR of grid cells varies from over 0.8 in the Appalachians to below 0.2 in

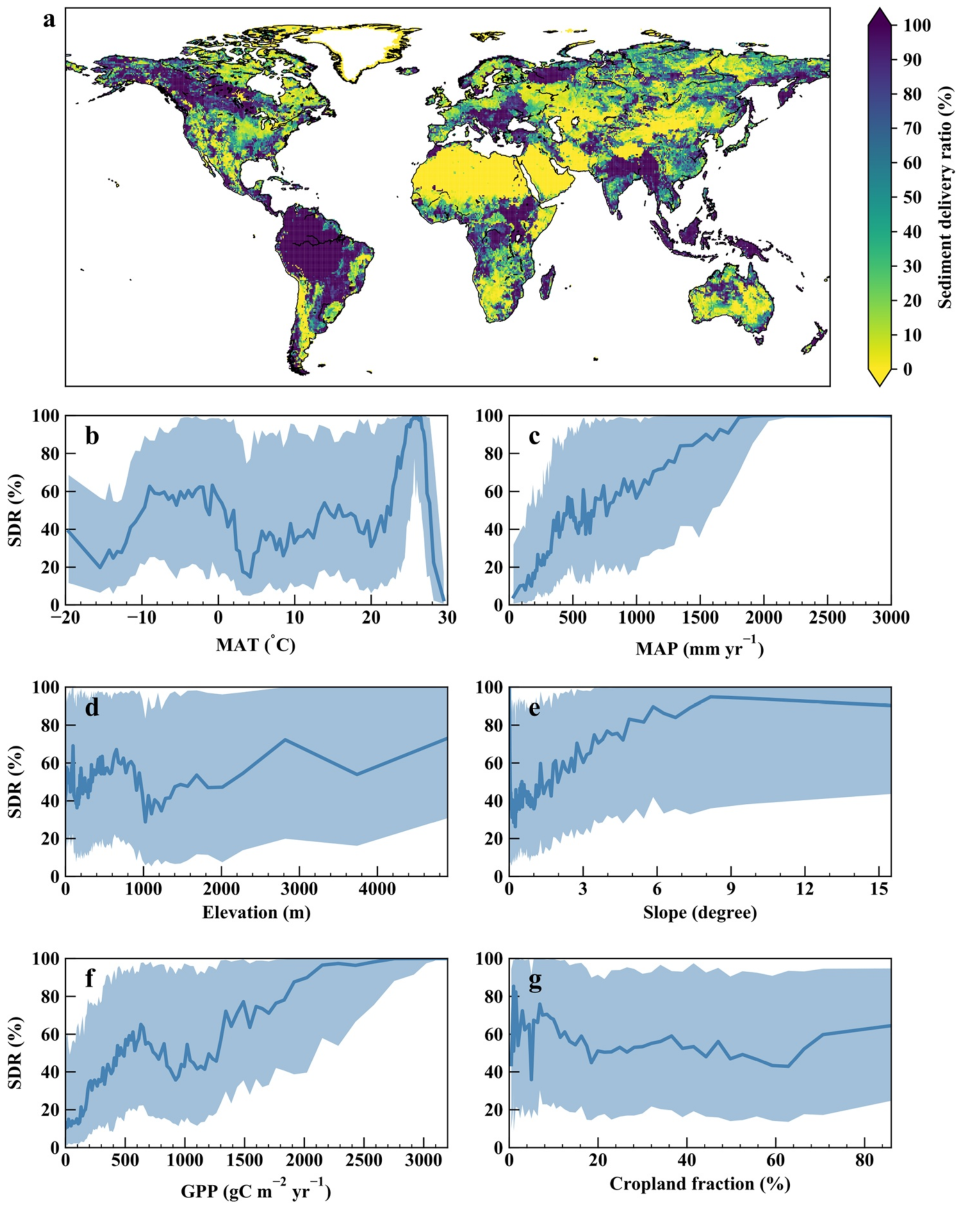

Figure 11. (a) Map of the simulated sediment delivery ratio, (b) relationships between sediment delivery ratio (SDR) and MAT, (c) MAP, (d) elevation, (e) slope, (f) GPP, and (g) cropland fraction. Solid lines and shaded areas in panels (b–g) represent the median and the 25th and 75th percentiles of the simulated SDR.

the Midwest plains within the Mississippi. Our SDR estimates for the Mississippi's subbasins that are calculated based on the basin-scale soil erosion and sediment flux are consistent with those used by the USDA's Conservation Effects Assessment Project (Arnold et al., 2014), with higher values in the Ohio-Tennessee (0.39), Lower Mississippi (0.45) and Arkansas-White-Red (0.40) river basins and lower values in the Upper Mississippi river basin (0.17). The sediment routed down the hillslopes to the riverine system accounts for 15.3% of the total eroded soil in Europe (Borrelli et al., 2018). The estimated mean SDR of the Mississippi and Amazon are 0.31 and 0.41, respectively. This difference is expected because compared with the Mississippi, the Amazon has a much larger fraction of forest coverage that limits soil erosion. Similar to the Amazon, other tropical rivers with high forest coverage also have larger SDR values, such as the Congo and many rivers in Southeast Asia (Figure 11). For these rivers, the high SDR values could imply that their sediment flux is erosion limited and thus more sensitive to LULCC, such as the expansion of economic crops, including soybeans and oil palms (Diodato et al., 2020).

Table 2
Comparison of the Simulated Change of Long-Term Sediment Flux Due to CA and LULCC and the Observed River Sediment Discharge Change (Meade & Moody, 2010) Since 1950s in the Mississippi and Its Major Subbasins

River basin	Sediment flux without CA and LULCC (Mt yr^{-1})	Sediment flux with CA and LULCC (Mt yr^{-1})	Simulated sediment flux change (Mt yr^{-1})	Observed sediment discharge change (Mt yr^{-1})
Mississippi	392	258	−134	−409
Missouri	98	55	−43	−236
Ohio	82	57	−25	
Upper Mississippi	56	34	−22	
Lower Mississippi	78	55	−23	
Tennessee	24	17	−7	
Arkansas-White-Red	53	39	−14	

The estimated SDR of grid cells exhibits diverse relationships with climate, topography, and vegetation (Figures 11b–11g). Generally, SDR has monotonically positive correlations with MAP and GPP, which could be explained by the limitation of soil erosion by dense natural vegetations. In contrast, SDR has a slightly negative correlation with cropland fraction, possibly because crop cultivation increases soil erosion substantially and transforms sediment flux over related river basins to transport limited. The positive relationship between SDR and slope indicates that with increasing land slope, sediment transport capacity increases faster than soil erosion.

Evaluating the impact of individual drivers, such as upland sediment flux, channel erosion/deposition and water management, on the change of river sediment flow (Cohen et al., 2014; L. Li et al., 2020) is not trivial. For example, the contributions of different drivers to the sediment reduction in the Mississippi river since 1950s are still uncertain (Meade & Moody, 2010; Mize et al., 2018; Murphy, 2020), even if river sediment has been routinely measured at the outlets of the river and its large subbasins. For the Mississippi, ELM-Erosion estimates that the sediment discharge under the pre-dam pre-conservation and post-conservation conditions are 392 Mt yr^{-1} (Mt = 10^6 *t*) and 258 Mt yr^{-1}, respectively (Table 2), which are very close to the previous estimates (400 and 253 Mt yr^{-1}, respectively) (Cohen et al., 2014; Milliman & Syvitski, 1992). As such, our model could be useful to constrain the partition of the Mississippi's sediment flow change. Comparing the full and no-CA-LULCC experiment, we estimate that the reduction of upland sediment flux caused by CA and LULCC might contribute to a third of the observed sediment flow reduction in the Mississippi, and within the Mississippi the sediment flux reduction in the Missouri is the most pronounced (Table 2). It implies that some channel sediment process, such as reservoir trapping, dominates the sediment flow reduction in the Mississippi, as claimed by Meade & Moody (2010).

4. Discussion

4.1. Global Soil Erosion and Sediment Flux Modeling

Our numerical experiments indicate that the regionalized parameter calibration scheme is effective in constraining the global soil erosion and sediment flux modeling and the calibrated ELM-Erosion has good skills in predicting the spatial variability of soil erosion and sediment flux at the global scale. For soil erosion, ELM-Erosion is consistent with the RUSLE-based benchmark data at the levels of pft, soil texture and climate classification, even though it uses input data at much coarser resolutions that are probably also at a lower quality. Comparison of the ELM-Erosion and RUSLE-based soil erosion to independent data shows that our model predicts more accurate relationships between soil erosion and topography in mountainous areas (elevation >1,000 m or slope >3°). This is possibly due to the large uncertainty in the slope length calculation in RUSLE and also uncertain dependence of soil erosion on slope length for regions of rough topography. Our analysis also shows that the land cover and hydrologic factors of ELM-Erosion have similar robustness to the land cover and rainfall erosivity factors of RUSLE in predicting the response of long-term soil erosion rates to vegetation and climate variations. Compared with WBMsed, ELM-Erosion may have improved the modeling of sediment flux in several aspects, including the elimination of unrealistic inland sediment flux hotspots, better representation of intra-basin sediment flux variations, and better representation of sediment flux in small river basins.

The improved ELM-Erosion provides several useful modeling capabilities that are rarely available in global soil erosion and sediment flux modeling but are important for understanding the soil erosion-climate feedbacks and the effects of soil erosion on aquatic and coastal ecosystems. For example, because ELM-Erosion couples soil erosion with the cycles of soil carbon and nutrients (Tan et al., 2020, 2021) and explicitly represents the factors of CA and LULCC, it can be used to better understand the constraint of soil erosion on the growth of food supplies and water quality in the developing countries under the changes of climate and land use. Also, because soil erosion and sediment flux are modeled simultaneously in ELM-Erosion, SDR can be easily estimated from the model simulations, which as demonstrated can be used to infer the potential sensitivity of river basins to environmental changes, such as climate change and LULCC. Further, by coupling it with the E3SM river sediment model that is now under development, ELM-Erosion will help to disentangle the mechanisms underlying the diverging trends of river water and sediment flows in many regions of the world (L. Li et al., 2020). Previous studies have shown that coastal wetland that receives insufficient sediment from inundation will be difficult to survive under accelerated sea-level rise (Kirwan et al., 2010) and the sediment supply of coastal wetland is profoundly impacted by river sediment dynamics (Blum & Roberts, 2009). As such, our synergistic effort to represent river sediment dynamics in conjunction with coupling of river and coastal sediment dynamics in E3SM will also advance understanding of coastal wetland evolution under global sea-level rise.

Our results show the importance to extending the practices of CA and managing irrigation to limit soil erosion. For countries that widely adopted the CA practices, such as US and Argentina, soil erosion in cropland has been reduced by over one-fourth. If the same techniques are applied to countries with rapid growth of population, such as countries in the Sub-Saharan Africa and South Asia, it would be possible to achieve the same amount of crop production despite the much lower soil loss and fertilizer applications, which would also benefit soil carbon sequestration (Lal, 2004). For irrigation, our study shows that it increases soil erosion in China and India by over 10%. As irrigation-induced soil erosion is positively correlated with irrigation supply, advanced irrigation techniques, such as drip irrigation, may also help reduce soil erosion.

4.2. Limitations and Future Work

Noticeably, the ELM-Erosion model still has several limitations that may contribute to errors of soil erosion and sediment flux simulations at the global scale. First, as the current ELM crop model only represents 10 crop pfts, soil erosion in cropland that cultivates erosion-prone crops may be underestimated. For example, our analysis shows that the underestimation of soil erosion over Australian cropland could be caused by the misrepresentation of several economic crops, such as sugarcanes, in ELM. Thus, future development may include the addition of more crop pfts such as those represented in the Community Land Model version 5.0 (Cheng et al., 2020). Second, our analysis indicates that soil erosion in regions of intense seismic activities is underestimated by ELM-Erosion. It is probably because the model does not represent landslide-induced soil erosion. Since landslides are a complex process related to soil micropore dynamics (Fan et al., 2017), it will be difficult to directly represent landslides in ESMs using process-based methods (Tan et al., 2018). Instead, it may be feasible to model landslide-induced soil erosion using physics-informed machine learning methods. Third, currently we apply a single CA factor to the equations of both rainfall-driven and runoff-driven soil erosion. But observations show that the CA practices may cause a lower ratio of rill to interrill erosion in cropland (Renard et al., 1997). Thus, it may be reasonable to apply different CA factors to the two erosion types. Fourth, because the current ELM does not assign soil columns to many of the land grid cells in Greenland and Antarctic, ELM-Erosion probably substantially underestimates sediment flux from glacial erosion (Overeem et al., 2017). Fifth, we used the pre-dam sediment yield from WBMsed to calibrate the sediment transport parameter c_3, assuming that upland sediment flux is equal to pre-dam sediment yield. But for some rivers, such as the Yellow River, upland sediment flux may not be balanced by river sediment discharge under the pre-dam condition, causing the accumulation or depletion of river channel sediment. In such cases, the simulated sediment flux could be biased. However, the WBMsed pre-dam data is almost the only data currently available for upland sediment flux benchmark at the global scale.

5. Conclusion

In this study, we explicitly represent the effects of cropland management actions (i.e., irrigation, conserved agriculture, and crop residue management) and geological factors (i.e., lithology and glacier) on soil erosion in ELM-Erosion to better predict the evolution of global soil erosion and sediment flux in the context of climate change and LULCC. To achieve a globally consistent model calibration, we apply a regionalized parameter calibration method. Compared with the RUSLE-based benchmark data, the new ELM-Erosion model shows consistent spatial variabilities at the levels of pft, soil texture and climate classification and performs better in predicting soil erosion in mountainous areas. Our experiments show that tillage and irrigation have profound impacts on soil erosion in cropland. For sediment flux, the ELM-Erosion and WBMsed simulations are consistent in inter-basin variability but have large differences in intra-basin variability for many rivers. The estimated SDR implies that areas with low sediment flux due to dense vegetation coverage may be sensitive to future changes in climate and land use. Our case study of the Mississippi river basin indicates that the change of upland sediment flux by CA and LULCC is not the dominant driver for the observed sediment flow reduction since 1950s in the basin. Overall, this study demonstrates that the developed model provides several useful capabilities that are important for understanding the soil erosion-climate feedbacks and the effects of soil erosion on aquatic and coastal ecosystems.

Data Availability Statement

The source code of ELM-Erosion, the model simulations and benchmark data are publicly available at https://doi.org/10.5281/zenodo.5762549.

Acknowledgments
The authors thank the reviewer and editor for their constructive comments. This research is supported by the Office of Science of the U.S. Department of Energy as part of the Earth System Modeling program through the Energy Exascale Earth System Model (E3SM) project. The Pacific Northwest National Laboratory is operated by Battelle for the U.S. Department of Energy under Contract DE-AC05-76RLO1830.

References

Adams, B. A., Whipple, K. X., Forte, A. M., Heimsath, A. M., & Hodges, K. V. (2020). Climate controls on erosion in tectonically active landscapes. *Science Advances*, *6*, eaaz3166. https://doi.org/10.1126/sciadv.aaz3166

Arnold, J. G., Harmel, R. D., Johnson, M. V. V., Bingner, R., Strickland, T. C., Walbridge, M., et al. (2014). Impact of the Agricultural Research Service watershed assessment studies on the conservation effects assessment project cropland national assessment. *Journal of Soil and Water Conservation*, *69*, 137A–144A. https://doi.org/10.2489/jswc.69.5.137a

Awulachew, S. B., McCartney, M., Steenhuis, T. S., & Ahmed, A. A. (2009). *A review of hydrology, sediment and water resource use in the Blue Nile Basin*. International Water Management Institute.

Batista, P. V., Davies, J., Silva, M. L., & Quinton, J. N. (2019). On the evaluation of soil erosion models: Are we doing enough? *Earth-Science Reviews*, *197*, 102898. https://doi.org/10.1016/j.earscirev.2019.102898

Beck, H. E., van Dijk, A. I. J. M., de Roo, A., Miralles, D. G., McVicar, T. R., Schellekens, J., & Bruijnzeel, L. A. (2016). Global-scale regionalization of hydrologic model parameters. *Water Resources Research*, *52*, 3599–3622. https://doi.org/10.1002/2015wr018247

Beck, H. E., Zimmermann, N. E., McVicar, T. R., Vergopolan, N., Berg, A., & Wood, E. F. (2018). Present and future Köppen-Geiger climate classification maps at 1-km resolution. *Scientific Data*, *5*, 180214. https://doi.org/10.1038/sdata.2018.214

Berhe, A. A., Barnes, R. T., Six, J., & Marín-Spiotta, E. (2018). Role of soil erosion in biogeochemical cycling of essential elements: Carbon, nitrogen, and phosphorus. *Annual Review of Earth and Planetary Sciences*, *46*, 521–548. https://doi.org/10.1146/annurev-earth-082517-010018

Blum, M. D., & Roberts, H. H. (2009). Drowning of the Mississippi Delta due to insufficient sediment supply and global sea-level rise. *Nature Geoscience*, *2*, 488–491. https://doi.org/10.1038/ngeo553

Borrelli, P., Alewell, C., Alvarez, P., Anache, J. A. A., Baartman, J., Ballabio, C., et al. (2021). Soil erosion modelling: A global review and statistical analysis. *Science of the Total Environment*, *780*, 146494. https://doi.org/10.1016/j.scitotenv.2021.146494

Borrelli, P., Robinson, D. A., Fleischer, L. R., Lugato, E., Ballabio, C., Alewell, C., et al. (2017). An assessment of the global impact of 21st century land use change on soil erosion. *Nature Communications*, *8*, 2013. https://doi.org/10.1038/s41467-017-02142-7

Borrelli, P., Robinson, D. A., Panagos, P., Lugato, E., Yang, J. E., Alewell, C., et al. (2020). Land use and climate change impacts on global soil erosion by water (2015–2070). *Proceedings of the National Academy of Sciences*, *117*, 21994–22001. https://doi.org/10.1073/pnas.2001403117

Borrelli, P., Van Oost, K., Meusburger, K., Alewell, C., Lugato, E., & Panagos, P. (2018). A step towards a holistic assessment of soil degradation in Europe: Coupling on-site erosion with sediment transfer and carbon fluxes. *Environmental Research*, *161*, 291–298. https://doi.org/10.1016/j.envres.2017.11.009

Campolongo, F., Cariboni, J., & Saltelli, A. (2007). An effective screening design for sensitivity analysis of large models. *Environmental Modelling & Software*, *22*, 1509–1518. https://doi.org/10.1016/j.envsoft.2006.10.004

Cheng, Y., Huang, M., Chen, M., Guan, K., Bernacchi, C., Peng, B., & Tan, Z. (2020). Parameterizing perennial bioenergy crops in version 5 of the Community Land Model based on site-level observations in the Central Midwestern United States. *Journal of Advances in Modeling Earth Systems*, *12*, e2019MS001719. https://doi.org/10.1029/2019ms001719

Cohen, S., Kettner, A. J., & Syvitski, J. P. (2014). Global suspended sediment and water discharge dynamics between 1960 and 2010: Continental trends and intra-basin sensitivity. *Global and Planetary Change*, *115*, 44–58. https://doi.org/10.1016/j.gloplacha.2014.01.011

Cohen, S., Kettner, A. J., Syvitski, J. P., & Fekete, B. M. (2013). WBMsed, a distributed global-scale riverine sediment flux model: Model description and validation. *Computers & Geosciences*, *53*, 80–93. https://doi.org/10.1016/j.cageo.2011.08.011

Compton, J. S., Herbert, C. T., Hoffman, M. T., Schneider, R. R., & Stuut, J. B. (2010). A tenfold increase in the Orange River mean Holocene mud flux: Implications for soil erosion in South Africa. *The Holocene*, *20*, 115–122. https://doi.org/10.1177/0959683609348860

CTIC. (2008). *Crop residue management survey*. Author. Retrieved from http://www.ctic.org/resourcedisplay/255/

Dadson, S. J., Hovius, N., Chen, H., Brian Dade, W., Hsieh, M.-L., Willett, S. D., et al. (2003). Links between erosion, runoff variability and seismicity in the Taiwan orogen. *Nature*, *426*, 648–651. https://doi.org/10.1038/nature02150

Davies-Colley, R. J., & Smith, D. G. (2001). Turbidity suspended sediment, and water clarity: A review. *Journal of the American Water Resources Association*, *37*, 1085–1101. https://doi.org/10.1111/j.1752-1688.2001.tb03624.x

Denman, K. L., Brasseur, G., Chidthaisong, A., Ciais, P., Cox, P. M., Dickinson, R. E., et al. (2007). Couplings between changes in the climate system and biogeochemistry. In S. Solomon, D. Qin, M. Manning, Z. Chen, M. Marquis, K. B. Averyt, et al. (Eds.), *Climate Change 2007: The Physical Science Basis. Contribution of Working Group I to the Fourth Assessment Report of the Intergovernmental Panel on Climate Change* (chapter 7, pp. 501–587). Cambridge University Press.

de Vente, J., & Poesen, J. (2005). Predicting soil erosion and sediment yield at the basin scale: Scale issues and semi-quantitative models. *Earth-Science Reviews*, *71*, 95–125. https://doi.org/10.1016/j.earscirev.2005.02.002

de Vente, J., Poesen, J., Verstraeten, G., Govers, G., Vanmaercke, M., Van Rompaey, A., et al. (2013). Predicting soil erosion and sediment yield at regional scales: Where do we stand? *Earth-Science Reviews*, *127*, 16–29. https://doi.org/10.1016/j.earscirev.2013.08.014

Dialynas, Y. G., Bastola, S., Bras, R. L., Billings, S. A., Markewitz, D., & Richter, D. D. (2016). Topographic variability and the influence of soil erosion on the carbon cycle. *Global Biogeochemical Cycles*, *30*, 644–660. https://doi.org/10.1002/2015gb005302

Diodato, N., Filizola, N., Borrelli, P., Panagos, P., & Bellocchi, G. (2020). The rise of climate-driven sediment discharge in the Amazonian River Basin. *Atmosphere*, *11*, 208. https://doi.org/10.3390/atmos11020208

Dirmeyer, P. A., Gao, X., Zhao, M., Guo, Z., Oki, T., & Hanasaki, N. (2006). GSWP-2: Multimodel analysis and implications for our perception of the land surface. *Bulletin of the American Meteorological Society*, *87*, 1381–1398. https://doi.org/10.1175/bams-87-10-1381

Doetterl, S., Van Oost, K., & Six, J. (2012). Towards constraining the magnitude of global agricultural sediment and soil organic carbon fluxes. *Earth Surface Processes and Landforms*, *37*, 642–655. https://doi.org/10.1002/esp.3198

Drewniak, B. A., Mishra, U., Song, J., Prell, J., & Kotamarthi, V. R. (2015). Modeling the impact of agricultural land use and management on US carbon budgets. *Biogeosciences*, *12*, 2119–2129. https://doi.org/10.5194/bg-12-2119-2015

Fan, L., Lehmann, P., McArdell, B., & Or, D. (2017). Linking rainfall-induced landslides with debris flows runout patterns towards catchment scale hazard assessment. *Geomorphology*, *280*, 1–15. https://doi.org/10.1016/j.geomorph.2016.10.007

Fick, S. E., & Hijmans, R. J. (2017). WorldClim 2: New 1km spatial resolution climate surfaces for global land areas. *International Journal of Climatology*, *37*, 4302–4315. https://doi.org/10.1002/joc.5086

Galy, V., Peucker-Ehrenbrink, B., & Eglinton, T. (2015). Global carbon export from the terrestrial biosphere controlled by erosion. *Nature*, *521*, 204–207. https://doi.org/10.1038/nature14400

García-Ruiz, J. M., Beguería, S., Nadal-Romero, E., González-Hidalgo, J. C., Lana-Renault, N., & Sanjuán, Y. (2015). A meta-analysis of soil erosion rates across the world. *Geomorphology*, *239*, 160–173.

Giardini, D., Grunthal, G., Shedlock, K. M., & Zhang, P. Z. (1999). The GSHAP global seismic hazard map. *Annals of Geophysics*, *42*, 1225–1230. https://doi.org/10.4401/ag-3784

Hartmann, J., & Moosdorf, N. (2012). The new global lithological map database GLiM: A representation of rock properties at the Earth surface. *Geochemistry, Geophysics, Geosystems*, *13*, Q12004. https://doi.org/10.1029/2012gc004370

Hurtt, G. C., Chini, L. P., Frolking, S., Betts, R. A., Feddema, J., Fischer, G., et al. (2011). Harmonization of land-use scenarios for the period 1500–2100: 600 years of global gridded annual land-use transitions, wood harvest, and resulting secondary lands. *Climatic Change*, *109*, 117. https://doi.org/10.1007/s10584-011-0153-2

Jenny, J. P., Koirala, S., Gregory-Eaves, I., Francus, P., Niemann, C., Ahrens, B., et al. (2019). Human and climate global-scale imprint on sediment transfer during the Holocene. *Proceedings of the National Academy of Sciences*, *116*, 22972–22976. https://doi.org/10.1073/pnas.1908179116

Jung, M., Reichstein, M., Margolis, H. A., Cescatti, A., Richardson, A. D., Arain, M. A., et al. (2011). Global patterns of land-atmosphere fluxes of carbon dioxide, latent heat, and sensible heat derived from eddy covariance, satellite, and meteorological observations. *Journal of Geophysical Research: Biogeosciences*, *116*, G00J07. https://doi.org/10.1029/2010jg001566

Kirwan, M. L., Guntenspergen, G. R., D'Alpaos, A., Morris, J. T., Mudd, S. M., & Temmerman, S. (2010). Limits on the adaptability of coastal marshes to rising sea level. *Geophysical Research Letters*, *37*, L23401. https://doi.org/10.1029/2010gl045489

Lal, R. (2004). Soil carbon sequestration impacts on global climate change and food security. *Science*, *304*, 1623–1627. https://doi.org/10.1126/science.1097396

Lanckriet, S., Araya, T., Cornelis, W., Verfaillie, E., Poesen, J., Govaerts, B., et al. (2012). Impact of conservation agriculture on catchment runoff and soil loss under changing climate conditions in May Zeg-zeg (Ethiopia). *Journal of Hydrology*, *475*, 336–349. https://doi.org/10.1016/j.jhydrol.2012.10.011

Lee, C. J., & Reutter, D. (2019). *Nutrient and pesticide data collected from the USGS National Water Quality Network and previous networks, 1963–2018*. U.S. Geological Survey Data Release.

Lehner, B., Verdin, K., & Jarvis, A. (2008). New global hydrography derived from spaceborne elevation data. *Eos, Transactions American Geophysical Union*, *89*, 93–94. https://doi.org/10.1029/2008eo100001

Leng, G., Leung, L. R., & Huang, M. (2017). Significant impacts of irrigation water sources and methods on modeling irrigation effects in the ACME Land Model. *Journal of Advances in Modeling Earth Systems*, *9*, 1665–1683. https://doi.org/10.1002/2016ms000885

Li, L., Ni, J., Chang, F., Yue, Y., Frolova, N., Magritsky, D., et al. (2020). Global trends in water and sediment fluxes of the world's large rivers. *Science Bulletin*, *65*, 62–69. https://doi.org/10.1016/j.scib.2019.09.012

Li, X., Niu, J., & Xie, B. (2014). The effect of leaf litter cover on surface runoff and soil erosion in Northern China. *PLoS One*, *9*, e107789. https://doi.org/10.1371/journal.pone.0107789

Lippe, M., Marohn, C., Hilger, T., Dung, N. V., Vien, T. D., & Cadisch, G. (2014). Evaluating a spatially-explicit and stream power-driven erosion and sediment deposition model in Northern Vietnam. *Catena*, *120*, 134–148. https://doi.org/10.1016/j.catena.2014.04.002

Lovelock, C. E., Cahoon, D. R., Friess, D. A., Guntenspergen, G. R., Krauss, K. W., Reef, R., et al. (2015). The vulnerability of Indo-Pacific mangrove forests to sea-level rise. *Nature*, *526*, 559–563. https://doi.org/10.1038/nature15538

Lu, H., Prosser, I. P., Moran, C. J., Gallant, J. C., Priestley, G., & Stevenson, J. G. (2003). Predicting sheetwash and rill erosion over the Australian continent. *Australian Journal of Soil Research*, *41*, 1037–1062. https://doi.org/10.1071/sr02157

Lugato, E., Smith, P., Borrelli, P., Panagos, P., Ballabio, C., Orgiazzi, A., et al. (2018). Soil erosion is unlikely to drive a future carbon sink in Europe. *Science Advances*, *4*, eaau3523. https://doi.org/10.1126/sciadv.aau3523

Meade, R. H., & Moody, J. A. (2010). Causes for the decline of suspended-sediment discharge in the Mississippi River system, 1940–2007. *Hydrological Processes*, *24*, 35–49.

Milliman, J. D., & Farnsworth, K. L. (2011). *River discharge to the coastal ocean: A global synthesis*. Cambridge University Press.

Milliman, J. D., & Syvitski, J. P. (1992). Geomorphic/tectonic control of sediment discharge to the ocean: The importance of small mountainous rivers. *The Journal of Geology*, *100*, 525–544. https://doi.org/10.1086/629606

Mishra, A. K., Placzek, C., & Jones, R. (2019). Coupled influence of precipitation and vegetation on millennial-scale erosion rates derived from ^{10}Be. *PLoS One*, *14*, e0211325. https://doi.org/10.1371/journal.pone.0211325

Misra, R. K., & Rose, C. W. (1996). Application and sensitivity analysis of process-based erosion model GUEST. *European Journal of Soil Science*, *47*, 593–604. https://doi.org/10.1111/j.1365-2389.1996.tb01858.x

Mize, S. V., Murphy, J. C., Diehl, T. H., & Demcheck, D. K. (2018). Suspended-sediment concentrations and loads in the lower Mississippi and Atchafalaya rivers decreased by half between 1980 and 2015. *Journal of Hydrology*, *564*, 1–11. https://doi.org/10.1016/j.jhydrol.2018.05.068

Montgomery, D. R. (2007). Soil erosion and agricultural sustainability. *Proceedings of the National Academy of Sciences*, *104*, 13268–13272. https://doi.org/10.1073/pnas.0611508104

Moosdorf, N., Cohen, S., & von Hagke, C. (2018). A global erodibility index to represent sediment production potential of different rock types. *Applied Geography*, *101*, 36–44. https://doi.org/10.1016/j.apgeog.2018.10.010

Morgan, R. P. C., & Duzant, J. H. (2008). Modified MMF (Morgan–Morgan–Finney) model for evaluating effects of crops and vegetation cover on soil erosion. *Earth Surface Processes and Landforms*, *33*, 90–106. https://doi.org/10.1002/esp.1530

Murphy, J. C. (2020). Changing suspended sediment in United States rivers and streams: Linking sediment trends to changes in land use/cover, hydrology and climate. *Hydrology and Earth System Sciences*, *24*, 991–1010. https://doi.org/10.5194/hess-24-991-2020

Oleson, K., Lawrence, D. B., Bonan, G., Drewniak, B., Huang, M., Koven, C., et al. (2013). *Technical description of version 4.5 of the Community Land Model (CLM). NCAR Technical Note NCAR/TN-503+STR*. NCAR.

Overeem, I., Hudson, B. D., Syvitski, J. P., Mikkelsen, A. B., Hasholt, B., Van Den Broeke, M. R., et al. (2017). Substantial export of suspended sediment to the global oceans from glacial erosion in Greenland. *Nature Geoscience*, *10*, 859–863. https://doi.org/10.1038/ngeo3046

Panagos, P., Borrelli, P., Poesen, J., Ballabio, C., Lugato, E., Meusburger, K., et al. (2015). The new assessment of soil loss by water erosion in Europe. *Environmental Science & Policy*, *54*, 438–447. https://doi.org/10.1016/j.envsci.2015.08.012

Pelletier, J. D. (2012). A spatially distributed model for the long-term suspended sediment discharge and delivery ratio of drainage basins. *Journal of Geophysical Research*, *117*, F02028. https://doi.org/10.1029/2011jf002129

Poesen, J., Nachtergaele, J., Verstraeten, G., & Valentin, C. (2003). Gully erosion and environmental change: Importance and research needs. *Catena*, *50*, 91–133. https://doi.org/10.1016/s0341-8162(02)00143-1

Poesen, J., & Savat, J. (1981). Detachment and transportation of loose sediments by raindrop splash: Part II detachability and transport ability measurements. *Catena*, *8*, 19–41. https://doi.org/10.1016/s0341-8162(81)80002-1

Powlson, D. S., Stirling, C. M., Jat, M. L., Gerard, B. G., Palm, C. A., Sanchez, P. A., & Cassman, K. G. (2014). Limited potential of no-till agriculture for climate change mitigation. *Nature Climate Change*, *4*, 678–683. https://doi.org/10.1038/nclimate2292

Prestele, R., Hirsch, A. L., Davin, E. L., Seneviratne, S. I., & Verburg, P. H. (2018). A spatially explicit representation of conservation agriculture for application in global change studies. *Global Change Biology*, *24*, 4038–4053. https://doi.org/10.1111/gcb.14307

Renard, K. G., Foster, G. R., Weesies, G. A., McCool, D. K., & Yoder, D. C. (1997). *Predicting soil erosion by water: A guide to conservation planning with the revised soil loss equation (RUSLE). Agriculture Handbook No. 703* (p. 404). U.S. Department of Agriculture.

Sacks, W. J., Cook, B. I., Buenning, N., Levis, S., & Helkowski, J. H. (2009). Effects of global irrigation on the near-surface climate. *Climate Dynamics*, *33*, 159–175. https://doi.org/10.1007/s00382-008-0445-z

Smets, T., Poesen, J., & Knapen, A. (2008). Spatial scale effects on the effectiveness of organic mulches in reducing soil erosion by water. *Earth-Science Reviews*, *89*, 1–12. https://doi.org/10.1016/j.earscirev.2008.04.001

Sobolev, S. V., & Brown, M. (2019). Surface erosion events controlled the evolution of plate tectonics on Earth. *Nature*, *570*, 52–57. https://doi.org/10.1038/s41586-019-1258-4

Syvitski, J. P. M., & Milliman, J. D. (2007). Geology, geography, and humans battle for dominance over the delivery of fluvial sediment to the coastal ocean. *The Journal of Geology*, *115*, 1–19. https://doi.org/10.1086/509246

Syvitski, J. P. M., Vörösmarty, C. J., Kettner, A. J., & Green, P. (2005). Impact of humans on the flux of terrestrial sediment to the global coastal ocean. *Science*, *308*, 376–380. https://doi.org/10.1126/science.1109454

Tan, Z., Leung, L. R., Li, H., Tesfa, T., Vanmaercke, M., Poesen, J., et al. (2017). A global data analysis for representing sediment and particulate organic carbon yield in Earth System Models. *Water Resources Research*, *53*, 10674–10700. https://doi.org/10.1002/2017wr020806

Tan, Z., Leung, L. R., Li, H.-Y., & Tesfa, T. (2018). Modeling sediment yield in land surface and Earth system models: Model comparison, development, and evaluation. *Journal of Advances in Modeling Earth Systems*, *10*, 2192–2213. https://doi.org/10.1029/2017ms001270

Tan, Z., Leung, L. R., Li, H.-Y., Tesfa, T., Zhu, Q., & Huang, M. (2020). A substantial role of soil erosion in the land carbon sink and its future changes. *Global Change Biology*, *26*, 2642–2655. https://doi.org/10.1111/gcb.14982

Tan, Z., Leung, L. R., Li, H.-Y., Tesfa, T., Zhu, Q., Yang, X., et al. (2021). Increased extreme rains intensify erosional nitrogen and phosphorus fluxes to the northern Gulf of Mexico in recent decades. *Environmental Research Letters*, *16*, 054080. https://doi.org/10.1088/1748-9326/abf006

Tang, J., & Zhuang, Q. (2009). A global sensitivity analysis and Bayesian inference framework for improving the parameter estimation and prediction of a process-based Terrestrial Ecosystem Model. *Journal of Geophysical Research: Atmospheres*, *114*, D15303. https://doi.org/10.1029/2009jd011724

USDA. (2018). *Summary report: 2015 National Resources Inventory*. Natural Resources Conservation Service, Center for Survey Statistics and Methodology, Iowa State University.

Vanmaercke, M., Poesen, J., Verstraeten, G., de Vente, J., & Ocakoglu, F. (2011). Sediment yield in Europe: Spatial patterns and scale dependency. *Geomorphology*, *130*, 142–161. https://doi.org/10.1016/j.geomorph.2011.03.010

Van Oost, K., Quine, T. A., Govers, G., De Gryze, S., Six, J., Harden, J. W., et al. (2007). The impact of agricultural soil erosion on the global carbon cycle. *Science*, *318*, 626–629. https://doi.org/10.1126/science.1145724

Wang, H., Yang, Z., Saito, Y., Liu, J. P., Sun, X., & Wang, Y. (2007). Stepwise decreases of the Huanghe (Yellow River) sediment load (1950–2005): Impacts of climate change and human activities. *Global and Planetary Change*, *57*, 331–354. https://doi.org/10.1016/j.gloplacha.2007.01.003

Wang, Z., Hoffmann, T., Six, J., Kaplan, J. O., Govers, G., Doetterl, S., & Van Oost, K. (2017). Human-induced erosion has offset one-third of carbon emissions from land cover change. *Nature Climate Change*, *7*, 345–349. https://doi.org/10.1038/nclimate3263

Wu, S., Chen, L., Wang, N., Zhang, J., Wang, S., Bagarello, V., & Ferro, V. (2021). Variable scale effects on hillslope soil erosion during rainfall-runoff processes. *Catena*, *207*, 105606. https://doi.org/10.1016/j.catena.2021.105606

Yue, Y., Ni, J., Ciais, P., Piao, S., Wang, T., Huang, M., et al. (2016). Lateral transport of soil carbon and land–atmosphere CO_2 flux induced by water erosion in China. *Proceedings of the National Academy of Sciences*, *113*, 6617–6622. https://doi.org/10.1073/pnas.1523358113

Zhou, T., Leung, L. R., Leng, G., Voisin, N., Li, H.-Y., Craig, A. P., et al. (2020). Global irrigation characteristics and effects simulated by fully coupled land surface, river, and water management models in E3SM. *Journal of Advances in Modeling Earth Systems*, *12*, e2020MS002069. https://doi.org/10.1029/2020ms002069

Reference From the Supporting Information

Kassam, A., Friedrich, T., Derpsch, R., & Kienzle, J. (2015). Overview of the worldwide spread of conservation agriculture. *Field Actions Science Reports*, *8*, 1–12.